Advances in Colloid and Interface Science 159 (2010) 144–159

Contents lists available at ScienceDirect

Advances in Colloid and Interface Science

journal homepage: www.elsevier.com/locate/cis

Impact of a heterogeneous liquid droplet on a dry surface: Application to the pharmaceutical industry

D.A. Bolleddula [a,*], A. Berchielli [b], A. Aliseda [a]

[a] University of Washington Department of Mechanical Engineering, Stevens Way, Box 352600 Seattle, WA 98195, United States
[b] Pharmaceutical Development, Pfizer, Inc., Global Research and Development, Groton Laboratories, Eastern Point Road MS 8156-35, Groton, CT 06340, United States

ARTICLE INFO

Available online 21 June 2010

Keywords:
Impact
Spreading
Colloidal dispersions
Tablet Spray coating

ABSTRACT

Droplet impact has been studied for over a hundred years dating back to the pioneering work of Worthington [1]. In fact, much of his ingenuity contributed to modern day high speed photography. Over the past 40 years significant contributions in theoretical, numerical, and experimental work have been made. Droplet impact is a problem of fundamental importance due to the wealth of applications involved, namely, spray coating, spray painting, delivery of agricultural chemicals, spray cooling, inkjet printing, soil erosion due to rain drop impact, and turbine wear. Here we highlight one specific application, spray coating. Although most studies have focused their efforts on low viscosity Newtonian fluids, many industrial applications such as spray coating utilize more viscous and complex rheology liquids. Determining dominant effects and quantifying their behavior for colloidal suspensions and polymer solutions remains a challenge and thus has eluded much effort. In the last decade, it has been shown that introducing polymers to Newtonian solutions inhibits the rebounding of a drop upon impact, Bergeron et al. [2]. Furthermore Bartolo et al. [3] concluded that the normal stress component of the elongational viscosity was responsible for the rebounding inhibition of polymer based non-Newtonian solutions. We aim to uncover the drop impact dynamics of highly viscous Newtonian and complex rheology liquids used in pharmaceutical coating processes. The generation and impact of drops of mm and μm size drops of coating liquids and glycerol/water mixtures on tablet surfaces are systematically studied over a range of $We \sim \mathcal{O}(1\text{–}300)$, $Oh \sim \mathcal{O}(10^{-2}\text{–}1)$, and $Re \sim \mathcal{O}(1\text{–}700)$. We extend the range of Oh to values above 1, which are not available to previous studies of droplet impacts. Outcomes reveal that splashing and rebounding are completely inhibited and the role of wettability is negligible in the early stages of impact. The maximum spreading diameter of the drop is compared with three models demonstrating reasonable agreement.

Contents

* Corresponding author.
E-mail addresses: dabolla@u.washington.edu (D.A. Bolleddula), aaliseda@u.washington.edu (A. Aliseda).

0001-8686/$ – see front matter © 2010 Elsevier B.V. All rights reserved.
doi:10.1016/j.cis.2010.06.003

1. Introduction

When a liquid drop orthogonally impacts a solid substrate, the drop may deposit into a thin disk, disintegrate into secondary droplets, or recede and possibly rebound and bounce, see Fig.1. When inertia is negligible the drop will deposit gently over the surface until equilibrium is reached. This equilibrium is a function of the solid/liquid/gas contact point commonly defined by the contact angle, θ. If the contact angle is at a minimum ($\theta=0$), the drop will spread indefinitely into a thin film, potentially reaching molecular thickness. If $\theta>0$, the drop will attain equilibrium once balance is reached between gravity, capillarity, and viscosity in a time of $\mathcal{O}(s)$. If the drop approached the substrate with sufficient kinetic energy, then the balance is complicated by the addition of inertia. When the surface/liquid combination has a high contact angle ($\theta>90°$) at equilibrium, then inertia will act to maintain excess surface energy upon impact and may partially recede the drop and even completely lift the drop off the surface. If the substrate is roughened, the drop may splash upon impact. Dimensional analysis provides a list of relevant parameters useful in discriminating drop impact outcomes,

$$We=\frac{\rho DU^2}{\sigma}, Re=\frac{\rho DU}{\mu},$$
$$Oh=\frac{\mu}{(\rho\sigma D)^{1/2}}=\frac{We^{1/2}}{Re}, K=WeOh^{-2/5}, \quad (1)$$

where ρ, μ, and σ denote the liquid density, viscosity, surface tension, respectively, and D and U are the initial drop diameter and impact velocity, respectively. *We*, *Re*, and *Oh* are the Weber, Reynolds, and Ohnesorge numbers, respectively, and K is a composite group that can be used to identify the onset of splashing. Gravity related effects are described through the Bond number $Bo=\rho gD^2/\sigma$ or by the Froude number $Fr=U^2/(gD)=We/Bo$. Usually, gravity effects are considered negligible in drop impact, yet this assumption is typically unsubstantiated. Two difficult parameters to model are roughness and wettability effects. These two parameters prove to be challenging in theoretical modelling yet are crucial to providing accurate boundary conditions at the contact line (i.e. three phase line or triple point, or interline).

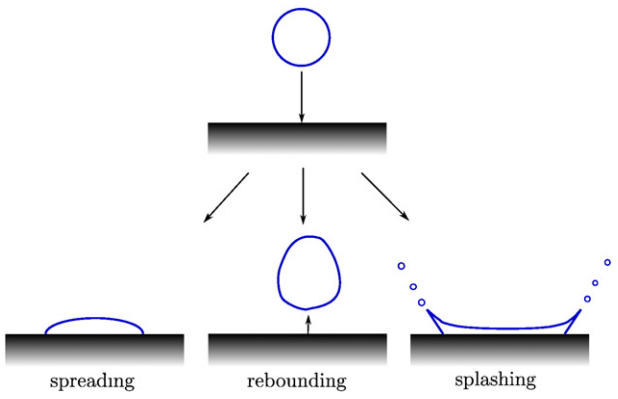

Fig. 1. Impact of a drop on a solid surface: spreading, bouncing, and splashing.

It is clear that dimensionless analysis provide a reduced set of components by which characterization can be simplified. Yet there remain many questions left unanswered. There must be a systematic methodology implemented in order to delineate potential outcomes. Some investigators have determined qualitatively the influence of various parameters such as viscosity, velocity, etc. and thereby determined their relative tendency to attain a specific outcome. It is still not clear whether dynamic similarity is held by the use of nondimensional parameters, [4]. It is also not clear if these parameters alone are sufficient in characterizing more complex rheological features, therefore further study is needed.

Drop impact studies are commonly motivated by their ubiquity in nature and industry. However, the overwhelming majority of the literature available has elucidated the behavior of pure liquids of low viscosity. This class of liquids is appropriate for the application towards the inkjet industry, agricultural sprays, or the aerospace industry. Pharmaceutical tablet spray coating processes typically contain liquids of complex rheology, containing large amounts of insoluble solids and considerably higher viscosities, $\mu>10$ cP. We are unaware of previous studies of droplet impact in the context of a range of parameters characteristic of spray coating processes utilized in the pharmaceutical industry to prepare tablet cores in final dosage form. It is our intention to provide a quantitative study of aqueous-based colloidal dispersions and their impact in a range of parameters characteristic of pharmaceutical coating operations.

Tablets are coated for various purposes including masking unpleasant taste, delivering a time released active agent, or brand recognition, [5]. A simplified schematic of the cross-section of a coating apparatus is seen in Fig. 2. An atomizer placed in the center of a rotating drum sprays droplets on the size range of $\mathcal{O}$(10–100 μm) at speeds of $U\sim$(1–10 m/s). The tablets tumble and are dried by a secondary flow of air. The coating process is a complex thermodynamic process yet at the tablet interface, droplets are impacted and may rebound, splash, or deposit cleanly as is desirable. An important question is how critical are the physical size of the droplets and impact speeds to deposition behavior. We hope to address that question in this study.

To date, solid and liquid surface impacts have been studied which has prompted two recent reviews on the subject, Rein [6] and Yarin [7]. Despite the numerous studies conducted to date, there is a gap in the knowledge regarding complex fluids which are used in industrial coating processes. The effects of surfactants in liquids led to the investigation of dynamic surface tension, Zhang and Basaran [8]. The introduction of polymers revealed that rebound can be completely suppressed which is explained by the elongational viscosity, Bergeron et al. [2]. The inkjet industry has benefitted significantly from drop impact studies such as Kannangara et al. [9] and Daniel and Berg [10]. These studies and more will be described in further detail in the following section with special attention to those relevant to coating fluids used in pharmaceutical industries.

The goal of this section is not to replicate the reviews mentioned above, but to provide background on some important concepts

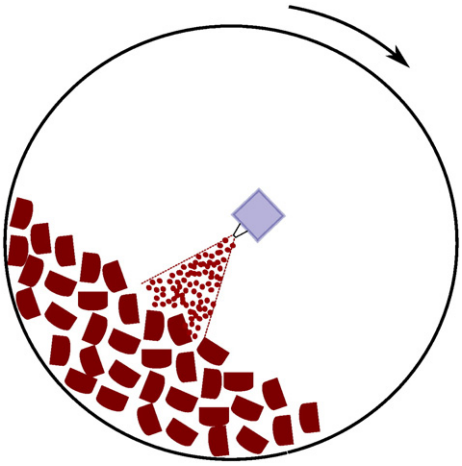

Fig. 2. Simple schematic of spray coating operation. Atomizer at the center sprays tablets as they are turned. Drying air (not shown) subsequently removes coating solvents for final film formation.

obtained from notable studies on droplet impact on dry surfaces published in the literature. We also aim at elucidating the need for accurate modelling considering non-Newtonian features. We will report a review of the studies conducted in three broad categories: spreading, splashing, and rebounding for Newtonian fluids. Subsequently, a survey of micron sized impact studies will be outlined. Finally, a review of impacts of complex fluids (multiple liquid phases, colloidal dispersions, and non-Newtonian characteristics) will follow. In the last section, we describe the experimental setup and experiments conducted and identify the response of industrial grade coating solutions in the pharmaceutical industry.

Four studies have been conducted and will be described in Section 3:

1. Determine rheology of coating liquids
2. Determine impact outcomes of pharmaceutical coating liquids in range of dimensionless groups indicative of these processes
3. Compare the effect of viscosity from coatings and glycerol/water mixtures
4. Determine utility of existing models that predict the maximum spreading diameter

2. Background and review

2.1. Spreading

2.1.1. Negligible inertia

When a drop is gently placed on a solid substrate, the balance of capillarity, gravity, and viscosity ensues. The *Bo* and the capillary number, $Ca = \mu U_{cl}/\sigma$, where U_{cl} is the velocity at the contact line, are typical parameters that describe the balance of forces. The wettability is defined by the contact angle. A simple horizontal force balance at the contact line gives us the well known Young's equation, Eq. (2)

$$\cos\theta = \frac{\sigma_{SG} - \sigma_{SL}}{\sigma_{LG}}. \tag{2}$$

If the surface is 'soft' and has low surface energy and the liquid has high surface tension the liquid will not spread indefinitely, but attain a shape of minimum area approximating a truncated spherical drop resting on the surface as shown in Fig. 3. The angle drawn in the liquid is defined as the contact angle, θ. The contact angle and surface tension of the liquid–gas interface are both measurable quantities but the quantity in the numerator of Eq. (2) is not. However, the magnitude of the numerator can be estimated from the known

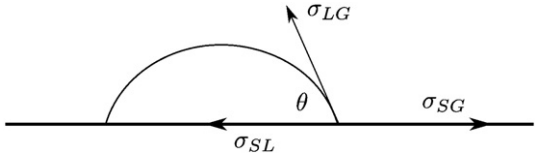

Fig. 3. Force balance at contact line.

contact angle and liquid surface tension. The solid surface energy has been estimated by the equations of Girifalco–Good and Fowkes which demonstrates attractive or repulsive forces, Berg [11]. The contact angle defined by Young's equation is defined at equilibrium. However, the angle attained when the three phase contact line is moved forward (advanced) or backward (receded) is a better indication of solid/liquid interfacial energies. The advancing and receding angle can be determined through many techniques, most notably the sessile drop method. The difference between the advancing angle, θ_{adv}, and the receding angle, θ_{rec} is defined as the hysteresis $\Delta\theta$. Causes for such hysteresis are attributed to surface roughness and chemical heterogeneity, de Gennes [12]. The time scale associated with these impacts can be considerably longer if $Ca<1$, being $O(s)$. Such experiments can be modelled using a lubrication approximation to the Navier–Stokes equations to yield an equation for the height of the drop. The results can be recast in terms of the spreading diameter, Starov et al. [13], Cox [14], and Hocking and Rivers [15].

Rioboo et al. [16] approximated the final diameter of a small drop on a surface with the inclusion of advancing and receding contact angles

$$\frac{d_i}{D} = 2\left[\frac{\sin^3\theta_i}{2(1-\theta_i)((2-\cos\theta_i-\cos^2\theta_i)}\right]^{1/3}, \tag{3}$$

where the subscript, *i*, denotes the advancing or receding contact angle. This formula is only valid for small drops, smaller than the Laplace length $\ell = \sqrt{\sigma/\rho g}$.

If gravity and viscosity are in balance, the radius of the drop $R \sim t^{1/8}$, Middleman [17]. If surface tension is included then the classical Tanner's law is derived, $R \sim t^{1/10}$, Tanner [18]. Both agree well with experimental data. It was also shown by Rafa et al. [19] that when non-Newtonian effects such as normal stress and shear thinning components are included, deviations from Tanner's law are minor and only require logarithmic corrections. Additional effects have been observed such as the thin precursor film of submicron dimensions which commonly is used to alleviate the force singularity at the contact line. Additionally, when this film is on the order of a few hundred Angstroms, van der Waals forces introduce additional interfacial forces commonly described as disjoining pressure. For further discussion of contact line related concepts see Dussan [20] and de Gennes [12].

2.1.2. Moderate inertia

When a drop impacts for $We \gg 1$, the impact is further complicated by the addition of inertia. Thus, the kinetic energy of the drop immediately before impact will play a determining role in the subsequent outcome. If the speeds are moderate and the surface is relatively smooth, the drop will spread out like a disc and come to rest as a truncated sphere or a thin film depending on the equilibrium contact angle of the system. As described before, the contact angle will still play a role in the final shape as the drop may recede and advance in an oscillatory manner until viscosity dampens the motion. The time scale of spreading associated with inertia is approximately D/U which yields milliseconds and μs for mm and μm sized drops, respectively. For partially wetting systems $\theta>0$, Chandra and Avedisian [21] observed entrainment of a small air pocket inside the drop upon

impact. Subsequently, van Dam and Clerc [22] used scaling arguments to describe the size of the bubble yielding a characteristic length, L_b as

$$L_b = \frac{\nu_{air}}{U_0}\left(\gamma_1^4 \frac{\rho}{\rho_{air}}\right)^{1/3}, \tag{4}$$

where γ_1 is an $\mathcal{O}(1)$ adjustable parameter. Agreement between experiments is quite reasonable. Medhi-Nejad et al. [23] simulated the impact of water, n-heptane and molten nickel droplets on a solid surfaces and verified the entrainment of an air bubble under the impacting droplet.

Although droplet impact affords significant experimental parameter space, the effort in modelling has promoted the use of a simple energy balance to predict the maximum spread of a droplet upon impact without splashing. Attané et al. [24] reviewed a large set of experimental data and contributed a new 1-D energy balance model to predict the dynamics of the spreading diameter. This approach dates back to Chandra and Avedisian [21] which will be outlined here.

2.1.3. Maximum spread: energy balance

The classical approach is to use an energy balance as follows

$$\underbrace{E_k + E_p + E_s}_{\text{before impact}} = \underbrace{E_k' + E_p' + E_s' + E_d'}_{\text{after impact}}, \tag{5}$$

and mass conservation

$$m = m'. \tag{6}$$

If splashing does not occur then work done by viscosity to dissipate energy is $E_d' = E_k + E_P + E_S$. The kinetic and surface energy before impact can be described by

$$E_k = \frac{1}{12}\rho U^2 \pi D^3, \tag{7}$$

and

$$E_s = \pi D^2 \sigma. \tag{8}$$

At maximum extension, the surface energy can be described by

$$E_s' = \frac{\pi}{4} D_{max}^2 \sigma(1-\cos\theta), \tag{9}$$

where the contact angle is defined herein at equilibrium.

The dissipated energy is difficult to determine since the velocity distribution inside the droplet is not known. This is the major modelling challenge which is still a topic of ongoing investigation, Roisman et al. [25], Roisman [26], Attané et al [24]. Chandra and Avedisian [21] used a very simple model to determine E_d'

$$E_d' = \int_0^{t_e}\int_V \phi dV\, dt \approx \phi V t_e. \tag{10}$$

The dissipation per unit mass of the fluid is given by

$$\phi = \mu\left(\frac{\partial u_x}{\partial y} + \frac{\partial u_y}{\partial x}\right)\frac{\partial u_x}{\partial_y} \approx \mu\left(\frac{U}{h}\right)^2, \tag{11}$$

where t_e is the characteristic time for deformation estimated to be $t_e \approx D/U$. The volume of the droplet when flattened out can be approximated by the shape of a disc as

$$V \approx \frac{\pi}{4} D_{max}^2 h, \tag{12}$$

where h represents the height of the disc. If we combine Eqs. (5)–(12), introducing the Re and We with $\beta_{max} = D_{max}/D$ and $E_p = E_p'$, the equation for the splashing deposition boundary is obtained

$$\frac{3}{2}\frac{We}{Re}\beta_{max}^4 + (1-\cos\theta)\beta_{max}^2 - \left(\frac{1}{3}We + 4\right) = 0. \tag{13}$$

From this equation one can obtain an expression for the maximum diameter. For coating liquids utilized in the pharmaceutical industry, viscosities are high, $\mu > 10$ cP and surface tensions are low $\sigma \sim 0.04$ N/m. In such circumstances, a balance between the initial kinetic energy $\rho D^3 U^2$ and viscous dissipation $\mu(U/h)D_{max}^3$ along with volume conservation $h \sim D^3/D_{max}^2$ yields $\beta_{max} \sim Re^{1/5}$ as remarked in Clanet et al. [27].

Experimental validation in Chandra and Avedisian [21] shows over-prediction of β_{max} which is attributed to the underestimation of the energy dissipated during droplet deformation. It is the viscous dissipation which continues to draw questions as to the validity in modelling. A simple model describing the force balance in squeezing of a cylinder under a mass yields an equation that can be fit to the regression group $(Re^2 Oh)^a$ with agreement within 10% of experimental data, Scheller and Bousfield [28]. Pasandideh-Fard et al. [29] derived the time to β_{max} as $t_\beta = 8D/3U$. Many authors have made assumptions to more accurately define viscous dissipation but often lack universality, Mao et al. [30], Asai et al. [31]. Most recently, Attané et al. [24] pursued the viscous dissipation term with vigor and collected the various approaches from the literature. In Attane's paper, he used the unsteady energy equation and listed two commonly used geometries at the maximum spread, the spherical cap, or cylinder. A second-order nonlinear differential equation describes the height of the drop with the use of an empirical function of the Oh number. The agreement is quite good using a diverse set of experimental and numerical data from the literature and expands upon previous work, predicting the dynamics of drop spreading. Mao et al. [30] used a stagnation point flow to model the flow distribution in the drop and developed a low and high viscous regime model for β_{max}. The model is fitted with a least squares regression to the data and is written as

$$\left[0.20Oh^{0.33}We^{0.665} + \frac{1}{4}(1-\cos\theta_{eq})\right]\beta_{max}^2 + \frac{2}{3}\beta_{max}^{-1} = \frac{We}{12} + 1. \tag{14}$$

The model of Mao et al. [30] which, like most models, only predicts the β_{max}, agrees within 10% of experimental data in the literature. Another later model by Asai et al. [31] provides a simple correlation

$$\beta_{max} = 1 + 0.48We^{0.5}\exp\left[-1.48We^{0.115}Oh^{0.21}\right], \tag{15}$$

ignoring the effect of the contact angle but still providing good agreement with their micron drop impact experiments. Roisman et al. [32] provide one of the few models that describe the rate of the spread and the maximum diameter without the use of any adjustable parameters. Roisman points out that the energy balance approach, does not reliably describe the flow in the impacting drop. Instead, a mass and momentum balance of the lamella and bounding rim which gives an expression for the dimensionless height of the drop and from conservation of mass yields the maximum diameter. In Roisman [26], a semiempirical relation based on this methodology was presented and is expressed as

$$\beta_{max} = 0.87Re^{1/5} - 0.40Re^{2/5}We^{-1/2}. \tag{16}$$

Furthermore, Roisman et al. [25] show that the flow accompanying drop impact is universal for high impact We and Re. Roisman et al. [32]

also accounts for the effect of receding and rebounding which will be discussed in the next section. For a further discussion of modelling, including the effect of solidification, see Bennett and Poulikakos [33].

The impact of water and glycerin on inclined smooth and wetted surfaces were studied in the work of Š. Šikalo et al. [34]. The critical *We* at which rebound occurs for a given impact angle was found to be constant if the normal velocity component is used in computing *We*. Effects of target curvature were studied in the work of Bakshi et al. [35]. From the film thickness developing over the target, they found three distinct temporal phases: drop deformation, inertia dominated, and viscous dominated. The first two phases were found to collapse onto each other for various *Re* and droplet–target combinations.

Numerical models have also provided insight into this problem, beginning with the earliest work where the full Navier–Stokes equations were solved using a Marker and Cell technique including the effect of compressibility, Harlow and Shannon [36]. Bechtel et al. [37] used a variational approach beginning with an energy balance and solved for the height of the drop as a function of *We*, σ_{air}/σ_{lg}, and μ. Fukai et al. [38] used a finite element approach with a deforming grid and a Galerkin method with defining features including the occurrence of droplet recoiling and mass accumulation. Subsequently, Fukai et al. [39] improved upon this model with the inclusion of wetting effects, including hysteresis $\Delta\theta$. Fard et al. [29] used a SOLA-VOF method and implemented measured values of dynamic contact angles as boundary conditions. Furthermore, Bussman et al. [40] used a 3-D model on a symmetric surface geometry with a volume tracking algorithm to track the free surface. Inviscid, axisymmetric spreading including σ and a boundary integral method was implemented by Davidson [41]. Pasandideh-Fard et al. [42] modelled the fluid dynamics, heat transfer, and phase change of a molten drop impact and solidification. The motivation for modelling was applied to controlling solidification of liquid metals in solder deposition of printed circuit boards.

2.2. Rebounding

When a drop impacts a surface with low wettability with $We \gg 1$, the drop will recede and potentially lift off the surface due to increased liquid/gas surface energy. Mao et al. [30] systematically studied this phenomenon and developed a model to predict the onset of rebounding. Recently, the manufacture of micron and even nano textured surfaces spurred the use of these surfaces in impact experiments. For a discussion of such surfaces and associated properties see Quéré [43]. Richard and Quéré [44] studied the bounding of water drops on micro textured surfaces. Okumura et al. [45] later used scaling arguments to predict the contact time upon maximum deformation and developed a model describing the flow field inside the drop. Renardy et al. [46] focused on the shape of the drop upon impact. They determined that when $We>1$ and $WeCa<1$ the drop takes on pyramidal shapes upon impact then forms a toroidal shape followed by lift off. The impact of low viscosity drops on superhydrophobic surfaces predicted a dependence on the maximum diameter of the drop as $\beta_{max} \sim D_0 We^{1/4}$, where D_0 is the initial drop diameter, Clanet et al. [27]. The dynamics of the contact angle has received little attention although it is expected to be important for this unsteady process. Bayer and Megaridis [47] focused on the dynamic behavior of the apparent macroscopic contact angle, θ_D for partially wettable systems. Validation with molecular kinetics of Blake and Haynes [48] was shown. Most recently, Kannan and Sivakumar [49] used water drops impacting on stainless steel surfaces comprising of rectangular grooves.

Modelling this behavior is complicated by the additional surface energy responsible for retraction of the drop. In Kim and Chun [50] an empirically determined dissipation factor is used to estimate viscous dissipation. The *Oh* is demonstrated to play the most important role in characterizing the recoiling motion. Using a level set approach, Caviezel et al. [51] developed a regime map for the conditions of rebounding and deposition.

2.3. Splashing

The interest in high speed impacts was applied to steam turbines and the aerospace industry in part to understand and prevent erosion of materials. Heyman [52] studied the impact of high speed liquid drops and determined parameters such as the impact pressure. Compressibility was explored further by Lesser [53]. In these impacts a shock wave moves into the liquid and solid. In these scenarios the liquid is treated as a compressible inviscid fluid. For more information on compressibility effects in high impact studies see Lesser and Field [54], Lesser [53], Dear and Field [55], Field et al. [56], and Rein [6].

Here we focus our discussion on $We<10^3$, neglecting compressibility effects. We define the outcome of splashing when a drop disintegrates into two or more secondary droplets after colliding with a solid surface. The criteria appropriately defining a splashing threshold are determined by the conditions at which the transition from spreading to splashing takes place. From our experience with rain, we see that high impact velocities yield splashes which points to kinetic energy playing a pivotal role. The surface energy acts as a restoring force and enables drops to break off in pursuit of a minimum energy state. The ratio of these two forces points to the importance of the *We* in defining splashing criteria. Other relevant variables include drop size, surface roughness, ambient gas pressure, surface compliance etc. Expressed in dimensionless groups, the criteria necessary for splashing are commonly defined as $K=f(WeRe^n)$ where the exponent n is determined through empirical correlations. The constant K is a function of the surface roughness and sets the value at which splashing or spreading occurs. The onset of splashing has been shown to depend on more than the fluid properties exclusively but it is still unclear how surface roughness plays a determinant role.

Stow and Hadfield [57] examined the splashing threshold of water drops. They found that drops spread without splashing as long as $RU^{1.69}<S_c$. S_c is a dimensional function of the properties of the liquid and the surface. In nondimensional form the relation can be written as $ReWe_c^2<\epsilon$ where $\epsilon=f(R_a)$, where R_a is the roughness amplitude. Mundo et al. [58] studied the deposition/splash limit and determined it to be $K=OhRe^{1.25}$. For rough surfaces at high *Re*, splashing is observed through the corona splash event. For low *Re* on rough surfaces deposition was observed. Furthermore a value of $K>57.7$ leads to incipient splashing where as $K<57.7$ leads to complete deposition. Range and Feuillebois [59] found splashing to be independent of viscosity (<10 cP) for low velocity impacts. The mechanism for the perturbations observed on the rim is explained by either surface roughness or a Rayleigh–Taylor instability. Droplet trains were studied by Yarin and Weiss [60] and provided measurement of secondary droplets which provided good agreement with their model. Cohen [61] developed a statistical model to describe the shattering of a single drop into multiple daughter drops neglecting viscosity. Bhola and Chandra [62] determined the shape of molten wax droplets falling on surfaces of varying temperatures finding that the substrate temperature was found to promote break-up. A model based on Rayleigh–Taylor instability was used to predict the number of satellite droplets that broke loose upon impact. Furthermore, Aziz and Chandra [63] studied the impact of molten metal droplets on heated substrates exploring the effects of solidification as well. Bussman et al. [64] simulated the fingering and splashing of a drop by introducing perturbations in the velocity of the fluid near the solid surface at a time shortly after impact. Splashing may be enhanced when a drop collides obliquely with a surface or when a drop impacts normally on a moving wall Bird et al. [65]. A theoretical approach to the determination of a splashing threshold was given by Cohen [61]. It is based on the assumption that there exists a minimum radius for secondary droplets. Rein [6] believed compressibility may play a more

dominant role in splashing and thus the Mach number must be included in analysis.

Rioboo and Tropea [4] delineated six different distinct outcomes following drop impact, the first being deposition as described earlier. The second is prompt splash where droplets are ejected directly at the contact line between the surface and the liquid. The third is the corona splash where a corona is formed during the spreading phase and eventually breaks into droplets. The receding break-up occurs when droplets are left on the surface during the retraction of the drop. Rebound occurs when the entire drop lifts off the surface and partial rebound when part of the drop stays attached to the surface. The unique descriptions of each distinct outcome are discussed in terms of individual properties as opposed to dimensionless groups. The two we will discuss in more detail are the prompt splash and corona splash.

Rioboo and Tropea [4] determined that the prompt splash is observed only with rough surfaces. This is attributed to the surface structure, namely the peaks which promote rupture and pinch off of thin ligaments formed upon initial spreading. The corona splash which is a more commonly seen splash in the studies of Range and Feuillebois [59], Bird et al. [65], and Yarin and Weiss [60] is produced when the rim of the droplet turns upward and subsequently breaks off into drops. This outcome is more characteristic of drop impact on liquid films. The receding break-up can be understood by wetting behavior. As the contact line recedes after reaching maximum spread, the dynamic contact angle decreases and when the minimum of $\theta_D = 0$ is reached the drops are left behind the bulk flow of the drop. It was concluded from his study that increasing the surface roughness, R_a, promotes a prompt splash. Increasing the impact velocity, U, also promotes a prompt splash and receding break-up. Xu et al. [66] showed prompt splashing to be initiated by surface roughness. For small drops deposition occurs and for large drops, corona splash is found on smooth surfaces and low surface tension liquids. Corona splashing was explained by instabilities produced by surrounding gas, Xu et al. [66]. Viscosity acts to reduce probability of all disintegration mechanisms. More recently it was shown by Xu et al. [67]. Moreover, Mandre et al. [68] demonstrated, by neglecting intermolecular forces, the liquid drop does not contact the solid, instead it spreads on a very thin air film. It is reasoned that the effect of viscosity acts to reduce probability of all disintegration mechanisms.

2.4. Micron sized experiments

It is worth to note some experiments which utilized realistic size droplets in the context of industrial applications. Asai et al. [31] developed a simple correlation for the maximum spread of inkjet droplets on various printing surfaces providing good agreement. Schiaffino and Sonin [69] studied the molten droplet deposition and solidification at low Weber numbers. Through scaling arguments, droplet impact was divided into four regimes based on *We* and *Oh* phase diagrams. The divisions identified dominant forcing regimes depending on the strength of capillarity, viscosity, and inertia. The generation of these drops is complicated by non-isothermal conditions associated with their production. Attinger et al. [70] followed this work and investigated the transient dynamics upon impact. The production of droplets is commonly created through the so called "drop-on-demand" mode. Basaran developed a new method to significantly reduce the drop radius without reducing the nozzle radius in Chen and Basaran [71]. The key to forming drops with $R_d < R$ is to judiciously control the capillary, viscous, and inertial time scales that govern the flow within the nozzle and eject a drop. van Dam and Clerc [22] studied water drops of 18 and 42 μm on glass substrates of varying wettabilities. In order to capture the dynamics upon impact of such a fast time scale $t \sim U/D \sim 10^{-6}$s, a delayed flash photographic technique was employed. Thus, the events from several drop impacts were sequentially ordered to observe the impact dynamics. The inherent assumption with this technique is that the impact is a highly repeatable event when the experimental conditions are precisely controlled. Higher spatial and temporal resolution was obtained by Dong et al. [72] using a pulsed laser and integrated with an imaging system. Furthermore, the drop-on-demand technique was expanded to the use of polymers in the work of Shore and Harrison [73]. Son et al. [74] studied the impact of water droplets on glass surfaces of varying wettabilities for $We = 0.05$–2 and $Oh = 0.017$. Following this study, the impact of Boger fluids, was observed in a range of $We = 2$–35 and $Oh = 0.057$. Tails were shown to follow the ejection of the droplet staying attached to the nozzle even upon impact, Son and Kim [75].

We are aware of only one study of the spreading of Newtonian and non-Newtonian drops which was solved numerically using the commercial code *Flow3D* Toivakka[76].

2.5. Complex rheology liquids

To this point, the discussion on impact has only included single component liquids. More complex solutions as may occur in industrial applications is the focus of the work here and a review of the relevant topics associated with such fluids will be described.

Surfactant solutions were investigated in a series of works relevant to spray coating operations since the liquid/gas interface undergoes rapid adjustments over a short time scale. The importance of these types of solutions comes with the ability of reducing surface tension and thereby enhancing spreading. The accumulation of surface active materials along the drop surface provides dynamic nature to the fluid interface and points toward the concept dynamic surface tension. Dynamic surface tension is a quantity commonly measured over a range of surfactant concentrations and typically decreases until a new lower equilibrium surface tension is reached. Surfactant solutions were studied in the work of Pasandideh-Fard et al. [29] where they explored the effect of equilibrium contact angle reduction. Surprisingly, they concluded that dynamic surface tension did not influence drop impact. However, Mourougou-Candoni et al. [77] concluded that droplet retraction was drastically influenced by the adsorption kinetics of the surfactants which limited the return to the equilibrium surface tension, σ. In a subsequent publication, Mourougou-Candoni et al. [78] observed two types of retraction: a fast destabilizing and an exponentially decaying slow retraction. The works of Basaran's group also studied the effects of surfactants, and σ_d, and reasoned that the decreases in surface tension thereby enhances spreading, yet in opposition is the non-uniform distribution of surfactants along the fluid interface giving rise to Marangoni stresses inhibiting spreading, Zhang and Basaran [8]. Emulsions drew attention from Prunet-Foch et al. [79] and it was determined that emulsification plays a significant role in the existence and aspects of splashing and also the shape of the contact line instabilities.

Bergeron et al. [2] discovered, by adding very small amounts of flexible polymers to an aqueous phase, inihibition of droplet rebound on a hydrophobic surface is attained, thus allowing desirable deposition behavior with minimal alteration of shear viscosity. The inclusion of small concentrations of polymers isolates the non-Newtonian effect to normal stress effects which can be quantified through the elongational viscosity, which explains the increased resistance to droplet rebound. Following this work, Cooper-White et al.'s [80] group systematically investigated the role of elasticity on the dynamics of drop impact. The quality of a Boger fluid is that the shear viscosity remains nearly constant thereby isolating the effect of the elasticity as the sole non-Newtonian feature. Worm like viscoelastic surfactant solutions were studied by Cooper-White et al. [80] with an outcome suggesting that lowering the equilibrium σ via surfactants normally offers little advantage over the time frame associated with impact, 5–10 ms for a 2–4 mm drop. The effect of strain hardening was included in Cooper-White et al. [81]. A unique hydrodynamic feature was included in Rozhkov et al. [82], where a polymer drop

Table 1
Summary of target surfaces and properties.

Surfaces	Notable properties
Acrylic	Synthetic polymer, PMMA
Mica	Silica mineral, molecularly smooth
Teflon	Synthetic fluoropolymer, PTFE
03136, 0% lubricant	100% microcrystalline cellulose
03134, 2% lubricant	Magnesium stearate
03135, 4% lubricant	Magnesium stearate

impacts a disc of diameter slightly larger than the drop. A splashing threshold was defined as

$$K_1 = \frac{\rho D^3}{\sigma t_{rel}} \times We^{3/8}, \quad K_1^* = 1140, \tag{17}$$

where t_{rel} is the relaxation time and when $K_1 > K_1^*$, splashing occurs. Four splashing regimes are discriminated in Rozhkov et al. [83]. Most recently, Bartolo et al. [3] derived an equation which identifies the elongational viscosity or more importantly, normal stress differences, for the reduction in rates of retraction and inhibition of rebounding behavior.

The impact and spreading of a neutrally buoyant suspension was investigated in Nicolas [84]. The study was conducted over a range of particle volume fractions and deduced that the particles are unevenly distributed throughout the drop with preference towards outer portion of the drop forming an annular structure. Furthermore, for large *Re*, splashing was observed and explained by additive role of particles.

We are aware of only one study of the impact of yield–stress liquids. Nigen [85] used a commercial vaseline as the major test fluid. The final shape of the drop depends on when the yield–stress limit is reached in the spreading phase.

3. Droplet impact experiments

We have demonstrated thus far from the review of literature, that there is an overwhelming body of work in pure liquid Newtonian drop impacts. Here it is our intention to focus our study on pharmaceutical grade coating solutions and thereby understand the influence of colloidal dispersions in spray coating operations. These coating liquids are aqueous suspensions and are commonly defined by their solid content by weight. It is noteworthy that the ratios studied here are realistic proportions for industrial scale coating operations. We will study three commercially available coating liquids from Colorcon, Inc. The three coating liquids are Opadry™II White differentiated by contents of partially-hydrolyzed polyvinyl alcohol (PVA), polyethylene glycol (PEG), hydroxypropyl methylcellulose (HPMC). The powders also consist of Lactose/TiO_2/Triacetin. The coatings are identified from here on by IDs #2, 4, and 5. Coatings #4 and 5 differ by the addition of PEG. It is important to note that these coating powders are lacking in polymer concentrations thus differentiating these liquids from previous studies where the dominant effect was a function of elasticity. A summary of these coatings and their physical properties are shown in Table 3. Coatings are prepared by slowly adding solid content to water over a magnetic stir plate. Care is taken to avoid aggregation of colloidal particles and obtain uniformity. Also, these coatings do not contain iron or other magnetic species with potential to remove solids from the liquid by the stir bar. The resulting liquid forms an aqueous suspension of colloidal particles that are fully wet by the dispersion medium. We will also use glycerol/water mixtures as test liquids to compare the effect that the colloids have on spreading rates.

The target surfaces are tablets (cores) identified by IDs 03136, 03134, and 03135 corresponding to 0, 2, or 4% hydrophobic lubricant (Magnesium stearate). We will also use pure smooth surfaces as a benchmark for comparison with the results of the impact on tablets. See Table 1 for a list of liquid/surface combinations studied and corresponding equilibrium contact angle. From here on we will discuss the coatings and surfaces by their IDs defined above. In all three studies we will characterize the effects by two parameters: the spreading diameter $\beta(t)$ and the centerline height of the drop $h(t)$. In this study we will provide fluid properties of coating liquids and then systematically study the impact on surfaces of varying wettabilities. The presentation of results will be divided into three sections: Experimental setup, Data, and Analysis.

3.1. Experimental setup

Fig. 4 is a schematic of our experimental apparatus. A high speed camera Phantom V12, Vision Research Inc., is used to visualize the impact of a drop from a solid surface. The magnification provides a spatial resolution of 17 μm/pixel and 1.45 μm/pixel for the mm and μm sized droplets, respectively. A long distance microscopic lens provided by Infinity USA Inc. is utilized in the micron sized drop impacts. The impact is backlit by an Edmunds fiber optic light source. Single mm size drops are ejected by a syringe pump through a stainless steel needle (22 g) and fall under their own weight with a diameter, $D \sim 2.5$ mm. The vertical and horizontal diameters are measured and an equivalent diameter is calculated by $D_{eq} = (D_h^2 D_v)^{1/3}$. The impact velocities are measured by the distance travelled of minimum location of the drop before and after impact. The uncertainty in this measurement is 0.13 m/s and 0.09 m/s for mm and μm sized impacts, respectively. The height of release is adjusted to obtain different velocities. The use of a piezoelectric sleeve bonded

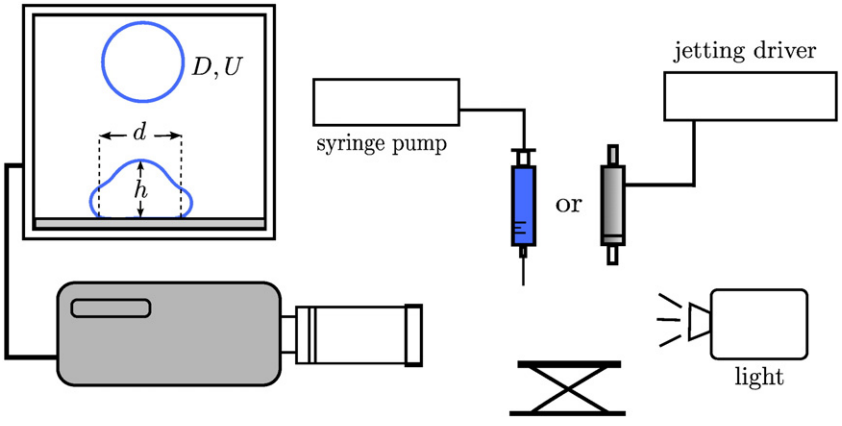

Fig. 4. Schematic of experimental apparatus. Data extracted is spreading diameter $d(t)$ and centerline height $h(t)$.

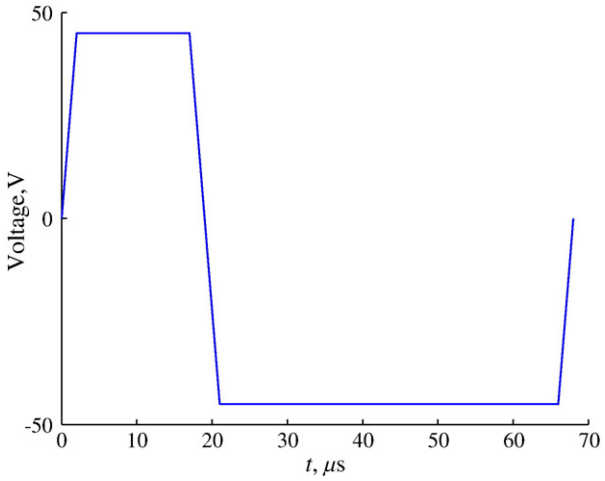

Fig. 5. Typical waveform used to eject droplets from nozzle. Frequencies vary but range from 10 to 100 Hz.

to a capillary tube of diameter 120 μm provides drops of size $\mathcal{O}$(60–80 μm). The piezo nozzle and voltage generator are provided by MicroFab, Inc. A typical waveform to eject droplets is shown in Fig. 5. In a typical experiment, mm and micron drop impacts are recorded at 7600 fps and 60000 fps, respectively. In order to obtain greater temporal resolution a higher speed camera is necessary to resolve short term dynamics of μm sized impacts. We investigate the parameter space defined in *We* and *Oh* shown in Fig. 6. By working with such highly viscous fluids we are able to realize higher $Oh \sim O(1)$ numbers thereby extending the range of previous studies. All quantitative data is collected with image processing software developed by NASA, Spotlight Klemek and Wright [86].

3.2. Experimental data

3.2.1. Impact surfaces

Table 1 summarizes the target surfaces utilized in this study. We have three tablet core substrates of varying hydrophobicities that are used as our impact targets as well as three ideal surfaces: acrylic, mica, and teflon. The tablets are Microcrystalline cellulose and are formed by compression. The surface of the tablets is altered by hydrophobic lubricant yet still can be subject to capillary imbibition. The use of highly viscous coating suspensions prevents penetration for the coating suspensions but not for the glycerol/water mixtures. Three 'ideal' surfaces are chosen based on their matched wettability with coating/tablet combinations (see Table 2). Impact of glycerol mixtures is attempted only on ideal surfaces.

Table 2
Summary of equilibrium contact angles from FTÅ200 measurement system.

Fluid	Mica	Acrylic	Teflon	3136	3134	3135
2, 20%, Opadry™II White, PVA/PEG (85F18422)	28	62	77	34	58	91
4, 15%, Opadry™II White, HPMC/PEG (33G28523)	15	54	75	33	62	87
5, 10%, Opadry™II White, HPMC (OY-LS-28914)	13	53	81	36	56	91
5, 12%, Opadry™II White, HPMC (OY-LS-28914)	13	49	75	40	70	92
5, 15%, Opadry™II White, HPMC (OY-LS-28914)	25	46	74	57	77	106
60% glycerol/H_2O	7.5	66	94			
75% glycerol/H_2O	13	75	92			
85% glycerol/H_2O	16	70	93			

3.2.2. Rheology

Characterization of the coating suspensions was carried out through shear viscosity measurements. A Brookefield II Cone + plate viscometer and an Anton Paar MCR301 Rheometer with a double gap configuration was utilized. Fig. 7 shows a typical viscosity measurement over a range of shear rates of 10^{-3}–$10^{3}s^{-1}$ for #5.

The shear viscosity maintains a very slight shear thinning profile for all coating suspensions used in this study and thus the implementation of the shear viscosity at 1000 s^{-1} is a conservative estimation. The shear rates upon impact can range from 1 to 1000 s^{-1}, thus employing the lowest viscosity serves as a first order approximation and is used herein. The viscosity can be fit excellently to the form $\mu = m\dot{\gamma}^{n-1}$ for $\dot{\gamma} > 1$. Furthermore, the viscosity at 1000 s^{-1} versus increasing solid content obeys an exponentially increasing function as observed in Fig. 8. Assessing if any non-Newtonian feature is present over the range of shear rates indicative of impact regimes is challenged by the coatings composition containing colloids of varying size, shape, and ability to aggregate. It is proposed that using the shear viscosity is an appropriate first characterization of these coating solutions. However we anticipate further characterization is necessary to gain quantitative understanding of the influence of colloidal particles in spreading. To date we are aware of only one quantitative study on the impact of a suspension of density matched particles by Nicolas [84].

The surface tension is measured with a du Nuoy Ring method and maintains a value approximately half that of water. Table 3 shows a

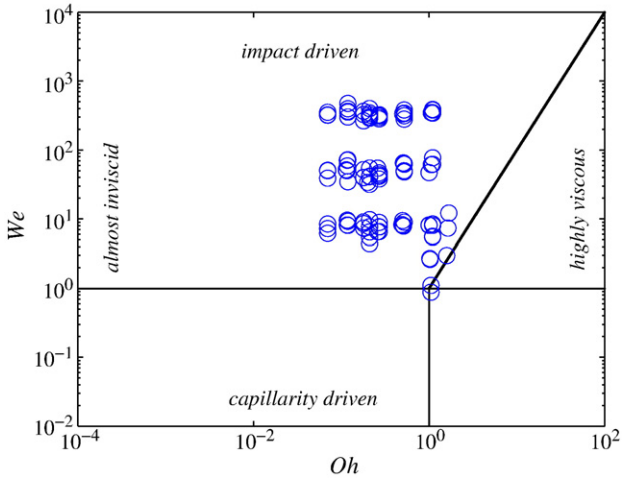

Fig. 6. Regime plot impact study based on *We* and *Oh*.

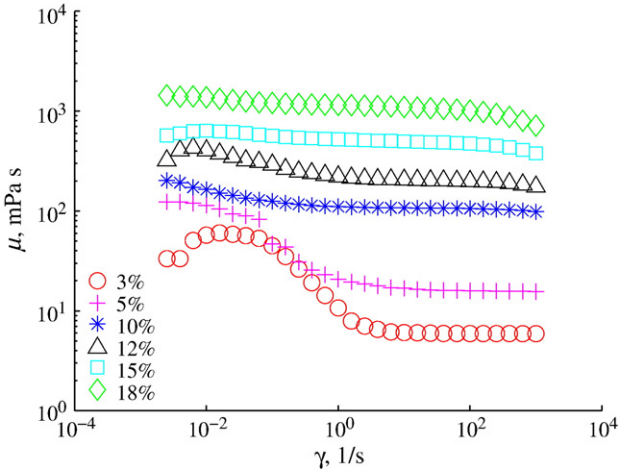

Fig. 7. Shear viscosity of Opadry suspension #5.

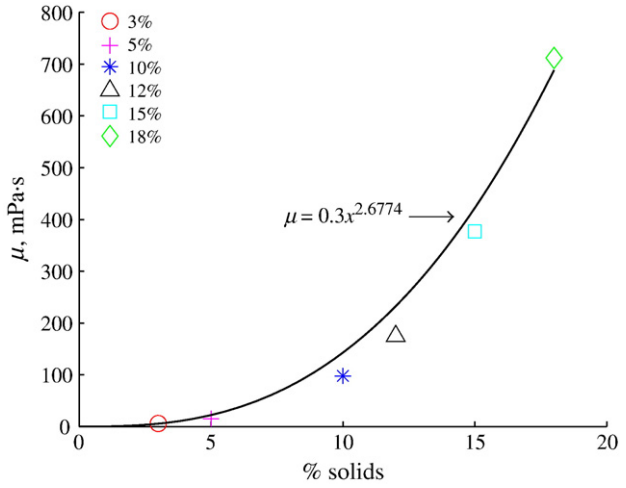

Fig. 8. Shear viscosity of Opadry suspension #5 taken at 1000 s^{-1} versus solid content.

summary of the fluid properties used to define dimensionless parameters.

3.2.3. Micron droplet ejection

Although it was demonstrated that gravity has only a minor effect in droplet impacts, it was only validated for low viscosity liquids, with $Oh \sim 10^{-2}$ [87]. We anticipate that gravity will also be negligible here, at least for μm size drops where $Bo \ll 1$. However, when mm size drops are employed then $Bo \sim 1$. Many authors justify neglect of gravity by introducing the Froude number expressed as $Fr = U^2/Dg \gg 1$ for both mm and μm size drops. This is not an accurate parameter to characterize the effect of gravity. The *Fr* characterizes the propagation of gravity surface waves against the convective fluid motion, whereas the key effect of gravity is to modify the overall shape of the droplet through the balance between potential, kinetic and surface energy.

Here we utilize viscosities of $\mathcal{O}(10^2$ cP) thus obtaining $Oh \sim 1$. Drop-on-demand technology has generally been motivated by the inkjet industry, yet the need for developing polymer based electronics such as polymer LED's has provided a need to generate micron size drops of more complex rheology liquids [75]. Here we demonstrate that by applying a suitable waveform and frequency we are able to generate 30–80 μm diameter drops with glycerol/water mixtures and coating #5, 10% solids both having $\mu \sim 100$ cP. A sample sequence of ejection of coating #5, 10% solids from the piezo nozzle is shown in Fig. 9.

At this point, the generation of micron sized droplets is produced at the expense of droplet speed and thus we are limited to $We \sim 1$ for micron drop impacts. Furthermore, limited temporal resolution of our high speed technology precludes us from obtaining precise dynamic behavior of the impacted droplet. However we are able to obtain the maximum spreading diameter which will be highlighted later. The ejection of higher speed droplets will be the focus for future work. From here on we focus our attention on experiments from mm size drop impacts.

Table 3
Summary of fluid properties.

Fluid	μ, mPa s @1000 s^{-1}	ρ, kg/m^3	σ, N/m	T, °C
2, 20%, Opadry™II White, PVA/PEG (85F18422)	39.35	1070	0.04393	25.4
4, 15%, Opadry™II White, HPMC/PEG (33G28523)	73.6	1040	0.04707	25.4
5, 10%, Opadry™II White, HPMC (OY-LS-28914)	98	1020	0.04822	25.4
5, 12%, Opadry™II White, HPMC (OY-LS-28914)	175	1030	0.04766	25.4
5, 15%, Opadry™II White, HPMC (OY-LS-28914)	377	1040	0.04667	25.4
60% Glycerol/H_2O	10.8[a]	1156	0.065	25.4
75% Glycerol/H_2O	35.5	1195	0.063[b]	25.4
85% Glycerol/H_2O	109	1220	0.062	25.4

[a] Viscosities for 60 and 75% glycerol/water are extracted from properties table.
[b] Interpolated value between 85% and 75% glycerol/water.

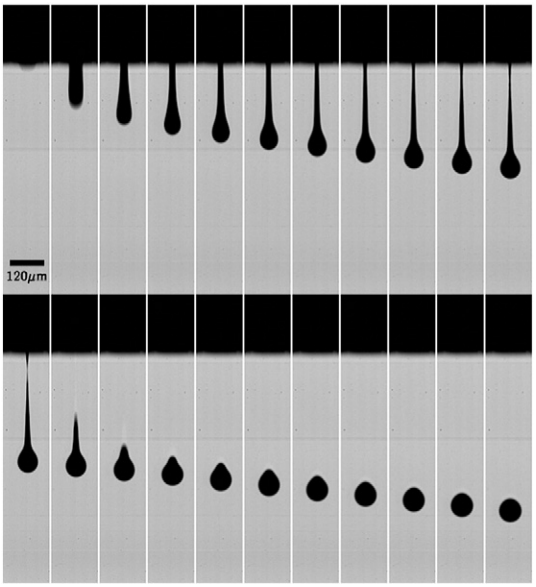

Fig. 9. Ejection sequence of #5, 10%. Time interval between each frame is 31 μs.

3.3. Analysis

Since the viscosities of the liquids we use in this study are high ($\mu > 10$ cP), splashing and rebounding is absent under the range of impact velocities (0.4–2.5 m/s) studied herein. Therefore we are able to quantify the outcome in terms of the spreading regime and extract the spreading diameter and centerline height of the drop during initial impact times, $\sim D/U$. A typical impact sequence is shown in Fig. 10. A drop of high viscosity impacts and jets a lamella around the periphery of the drop and attains a 'mushroom' like shape for a few instants. Given sufficient kinetic energy, the apex of the drop overshoots the height of the rim then either oscillates or dampens into a flat disc or a spherical cap at equilibrium. The contact line region undergoes sharp adjustments in slope depending on the speed of the contact line. The liquid/solid area rapidly dissipates any available energy and settles to equilibrium in a matter of a few ms. Fig. 11 shows the dimensional results for spreading diameter and centerline height of the drop immediately following contact with the substrate. The general behavior of the spreading diameter, $d(t)$ follows a decaying

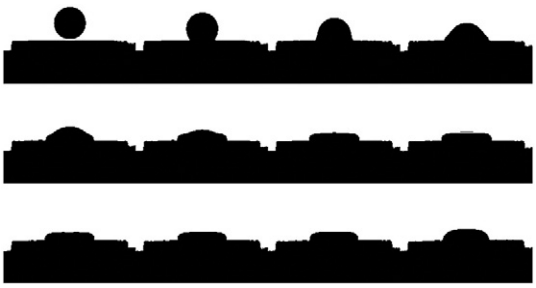

Fig. 10. Typical impact outcome. Time interval between each image is 0.2 ms excluding the last image which occurs approximately 11 ms after impact. Coating #5, 10% with $D \approx 2.5$ mm impacts tablet 03135 at velocity of $U = 2.47$ m/s.

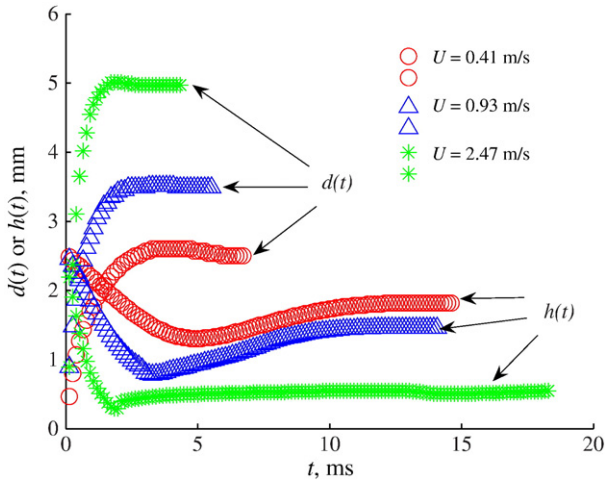

Fig. 11. Spreading diameter $d(t)$ and centerline height $h(t)$ taken after moment of impact for three different velocities. Coating #5, 10% impacts tablet 03135.

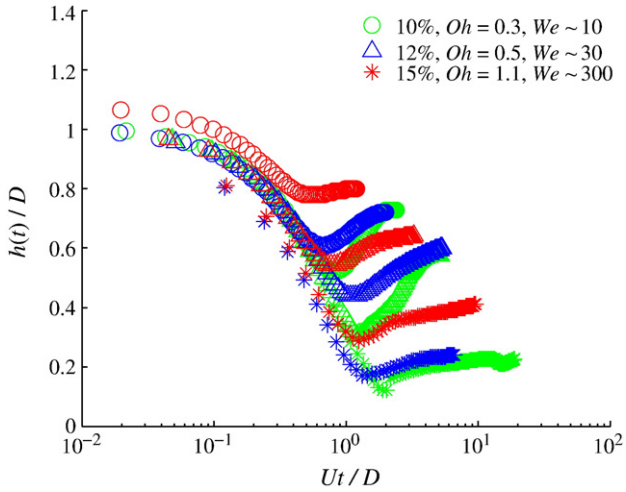

Fig. 13. Centerline height, of coating #5 (see Table 3) on tablet surface 03135 (4% lubricant). $h(t)/D$ versus time scaled with initial impact velocity U and diameter D. The colors green, blue, and red indicate 10, 12, and 15% solid content. The symbols ○,△, and * are for We of approximately 10,30, and 300, respectively.

exponential of the form $d(t) = d_{max}(1 - \exp[-ct])$, where c is presumable a function of fluid properties, e.g. surface tension, viscosity, etc. The centerline height also obeys a rapidly decaying exponential behavior for the first few ms and then slowly decays to equilibrium. From here on we will present the data in nondimensional form using the initial diameter and velocity of the drop D and D/U as the length and time scales, respectively.

The following studies will be discussed in terms of We, Oh, and Re. The regime plot shown in Fig. 6 describes the experimental space for $We \sim \mathcal{O}(1\text{–}400)$, $Oh \sim \mathcal{O}(10^{-2}\text{–}1)$, $Re \sim \mathcal{O}(1\text{–}700)$, and $Bo \sim \mathcal{O}(10^{-3}\text{–}1)$. This range captures the behavior of impact conditions in atomization experiments where impact speeds are $U \sim \mathcal{O}(1\text{–}10)$m/s. Noteworthy is the extension of $Oh \sim \mathcal{O}(1)$ which initiates a balance between viscosity and surface tension. From here on we will discuss the results in terms of these dimensionless groups. The spreading rate and centerline height are expressed in nondimensional form as $\beta(t) = d(t)/D$ and $h(t)/D$, respectively (see Fig. 4. Reproducibility of the following results is within 5% when comparing maximum diameters.

The focus of this effort will be divided into three parts. Firstly, we will characterize the behavior for three increasing amounts of solid content for a single coating. Secondly we will compare the behavior of the three coatings with varying solid contents. Finally, we will compare the coatings to three glycerol/water mixtures of similar viscosity to elucidate the effect of colloidal particles. For all studies, we will discuss the studies in terms of order of magnitude but for reference to exact parameters calculated see Table 4 in the Appendix.

3.3.1. Study 1. Characterization of solid content of coating #5

Fig. 12 demonstrates the effect of solid content (viscosity) on spreading. The viscosity decreases the spreading rate for all three We tested. Similarly, the height of the drop rapidly drops until a dimensionless time $\mathcal{O}(1)$ and subsequently viscosity dampens the motion of the drop into a slow decay to equilibrium, Fig. 13. In Fig. 14 we observe very little impact of the percentage of lubricant in the substrate composition on the spreading behavior. This was expected since we are only concerned with the impact dynamics for a dimensionless time of $\tau = Ut/D$ 1–4 for $We \sim 300$. Decreasing the impact speed verifies this expected behavior only showing a slight difference as observed in Fig. 15 for $We \sim 10$ where the interfacial energy at the solid/liquid area plays a more significant role. Increasing

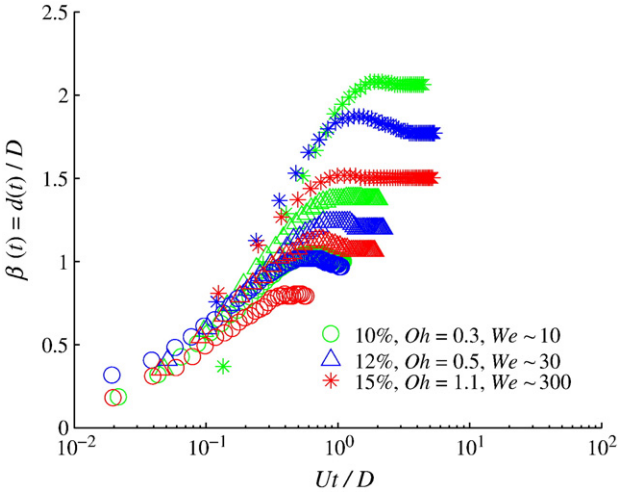

Fig. 12. Spreading diameter, β of coating #5 (see Table 3) on tablet surface 03135 (4% lubricant). β versus time scaled with initial impact velocity U and diameter D. The colors green, blue, and red indicate 10, 12, and 15% solid content. The symbols ○,△, and *are for We of approximately 10, 30, and 300, respectively.

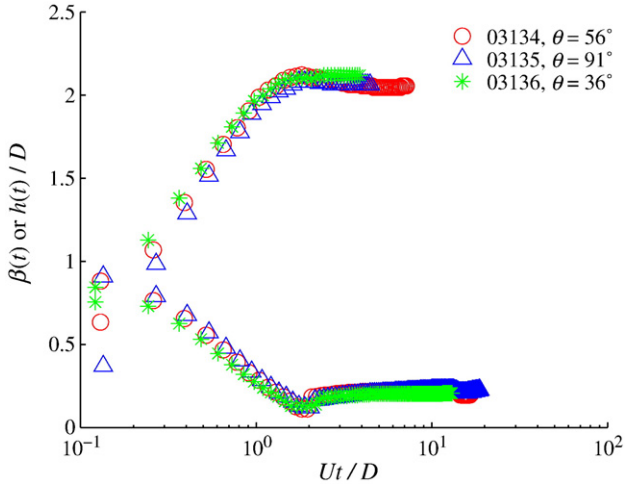

Fig. 14. Spreading diameter and centerline height on tablets of differing wettabilities for $We \sim 300$ coating #5, 10%. Top and bottom sets of curves describe β and h, respectively.

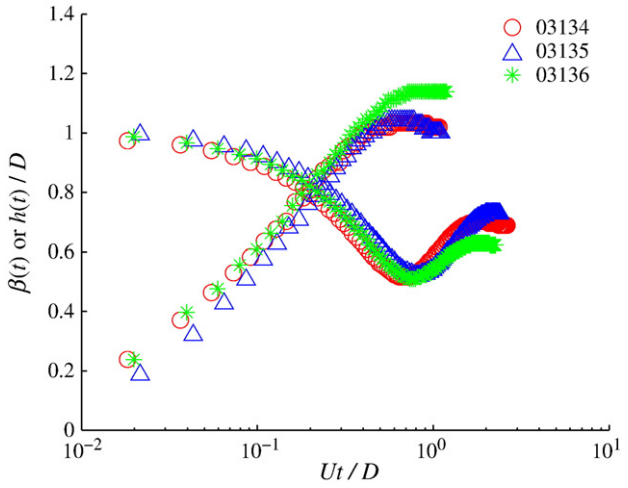

Fig. 15. #5 10%, Spreading diameter and centerline height on tablets of differing wettabilities for $We \sim 10$. Top and bottom sets of curves describe β and h, respectively.

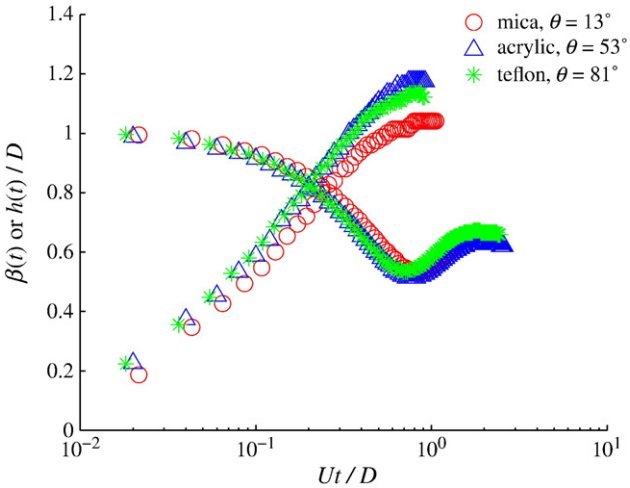

Fig. 17. #5 10%, Spreading diameter and centerline height on ideal surfaces of differing wettabilities for $We \sim 10$. Top and bottom set of curves describe β and h, respectively.

the solid content of #5 does not alter this trend as shown in Fig. 16. To further verify this conclusion, we observe the outcome on the ideal surfaces and find enhanced spreading for acrylic and teflon surfaces compared to mica in Fig. 17. It is reasoned that the higher surface energy of mica causes a delay during impact times. For $We \sim 300$, we see in Fig. 18 that acrylic shows faster spreading and confirms the negligible effect of wettability in the early stages of impact. Comparison of the two remaining coatings, #4 and #2 will reveal any variation in colloidal behavior during spreading.

3.3.2. Study 2. Comparison of coatings #5–10%, #4–15%, and #2–20%

Comparing the three coatings on tablet 03136 (no lubricant) in Fig. 19 we observe a slightly higher spread of coating #4 for $We \sim 10$ which is validated for $We \sim 300$ in Fig. 20. This trend is consistent for tablets 03134 and 03135. It is reasoned that although the solid content is larger (15% compared to #5, 10%), the addition of PEG may enhance spreading in the early stage of impact by acting as a surfactant. Moreover, the colloidal particles of #4 may not provide increased resistance due to addition of PEG which is absent from #5. Furthermore, it is apparent in Fig. 20 that coatings #2, 20% and #5, 10% follow similar paths despite the doubling of solid content and

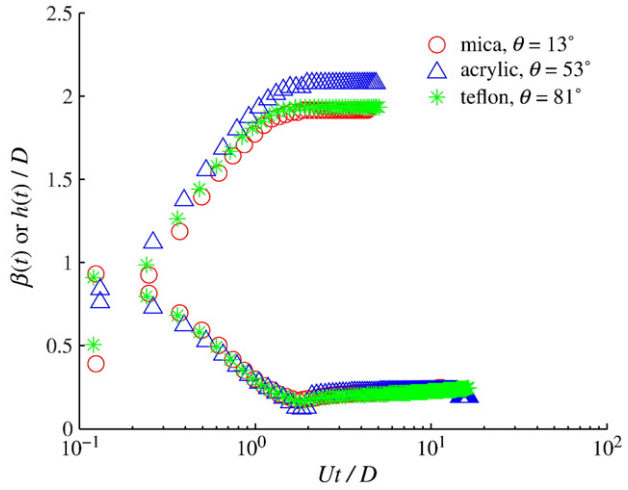

Fig. 18. #5 10%, Spreading diameter and centerline height on ideal surfaces of differing wettabilities for $We \sim 300$. Top and bottom sets of curves describe β and h, respectively. Note that the slightly large spread is observed on acrylic compared to mica but this is explained by statistical uncertainty between repeated tests.

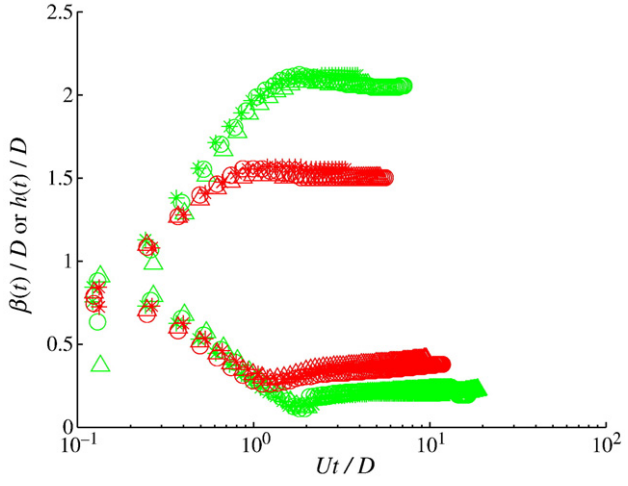

Fig. 16. Spreading diameter and centerline height on tablets of differing wettabilities for $We \sim 300$. Top and bottom sets of curves describe β and h, respectively. Green and Red sets of curves are for coatings #5, 10% and #5, 15%, respectively. The symbols ○, △, and * correspond to tablet surfaces 03134, $\theta = 56°$, 03135, $\theta = 91°$,and 03136, $\theta = 36°$, respectively.

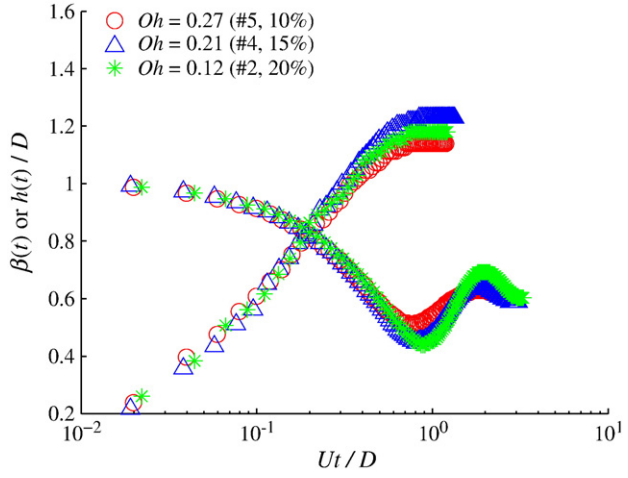

Fig. 19. Spreading diameter and centerline height for coatings #5, 10%, 4, and 2 for $We \sim 10$ on tablet 03136 (no lubricant). Top and bottom sets of curves describe β and h, respectively. Note that coating 4 obtains a higher spread but we confirm this observation by looking at a higher *We*.

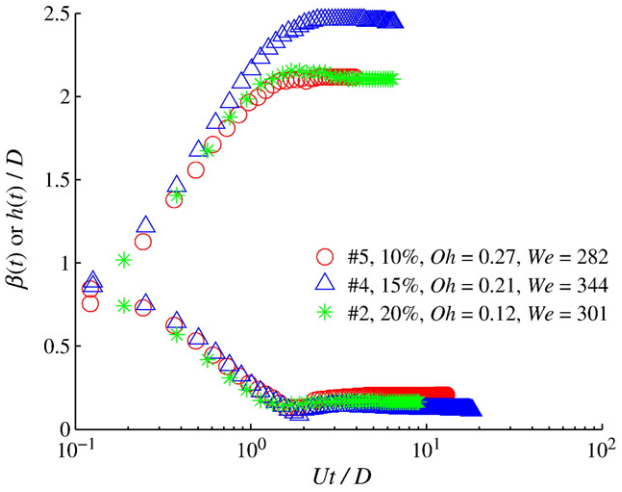

Fig. 20. Spreading diameter and centerline height for coatings #5, 10%, 4, and 2 for $We \sim 300$ on tablet 03136 (no lubricant). Top and bottom sets of curves describe β and h, respectively. Confirm large spreading diameter for coating 4.

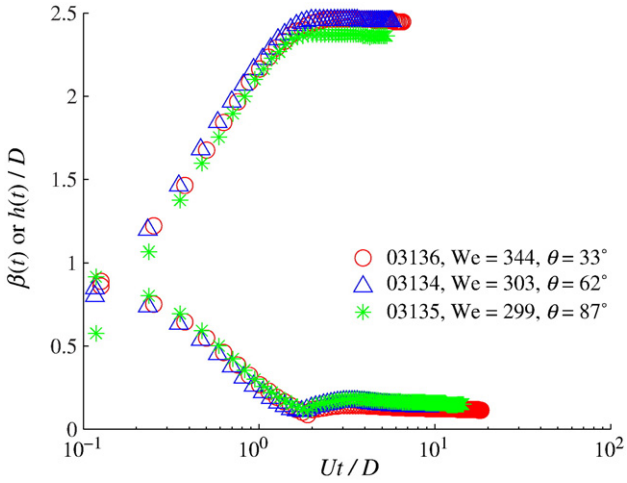

Fig. 22. Spreading diameter and centerline height for coating #4 on tablets for $We \sim 300$.

viscosities of 40 and 98 mPa s, respectively. These two contradictory effects cancel out in the spreading behavior.

Examining coating #4 15%, $Oh = 0.2$ in more detail, we observe a diminished spreading and slight recession of the diameter for $We \sim 10$ shown in Fig. 21. For $We \sim 30$, the centerline height overshoots the height of the rim and remains out of sight until it recovers over the rim and proceeds to go through two successively damped periods of oscillation. The linear portion which starts at 10° and ends approximately at 2.5 is the height of the rim data collected automatically from the image processing algorithm. The linear rise of the height of the rim (not the centerline) when the apex of the drop falls below is an unexpected trend and not previously documented to our knowledge. Note that this whole process occurs with an arrested contact line. This way of preserving conservation of mass is in opposition to the most common behavior where the decrease in centerline height is balanced by continued spreading until equilibrium is reached. Furthermore, the lack of this effect for $We = 300$ points toward a window of We where this behavior occurs.

If we compare the behavior of coating #4 on tablet and ideal surfaces we observe similar trends for all three tablet surfaces with the $\beta_{max} \approx 2.5$, Fig. 22. Fig. 23 demonstrates for $We \sim 300$, $\beta_{max} \approx 2.5$ on acrylic as opposed to mica and teflon attaining $\beta_{max} \approx 2$. At this point we have not compared the effect of the coatings to Newtonian liquids. It will be apparent how dominant the role of colloidal particles are by comparing the spreading behavior for the glycerol/water mixtures and coating liquids at similar viscosities.

3.3.3. Study 3. Comparison of coatings and glycerol/water mixtures

We compare the previous results to glycerol/water mixtures on ideal surfaces. Reduction in spreading rate is confirmed with the increase in viscosity as demonstrated in Fig. 24. The role of the colloids has been understated thus far but it will be apparent if they affect the spreading rate by comparing the glycerol/water mixtures to coating liquids. Since 85% glycerol/water and #5, 10% have viscosities of O (100 cP) we can compare their results over a range of We. Fig. 25 demonstrates the expected behavior in the role of colloidal particles promoting increased resistance to spreading as indicated by slightly larger Oh. Similarly in Fig. 26 for 75% glycerol/water and coating #2 we obtain increased spreading for the glycerol/water mixture. It is important to note that following the impact time scale ($Ut/D \sim 1$–4), the glycerol/water drops recede back to a shape obtaining contact angle equilibrium. Receding is minimal if even present for coating liquids which is explained by reduced surface tension compared to glycerol/water solutions and resistance of solid particles.

We have demonstrated that the colloidal dispersions show very slight differences in behavior with comparable pure Newtonian liquids. To further validate this observed behavior and verify the utility of previous models to include colloidal dispersions, we will

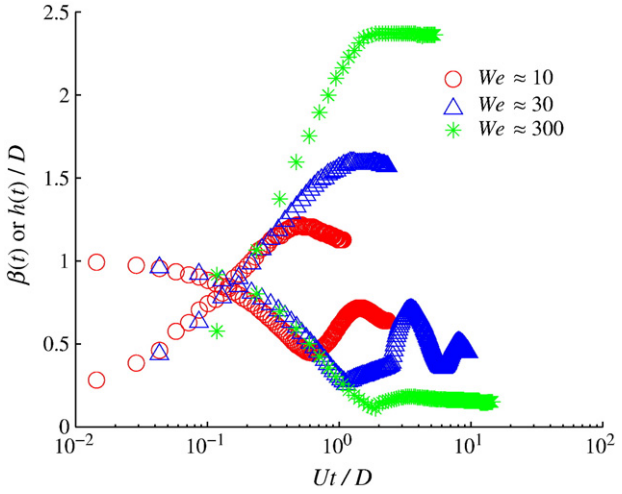

Fig. 21. Spreading diameter and centerline height for coating #4 on tablet 03135.

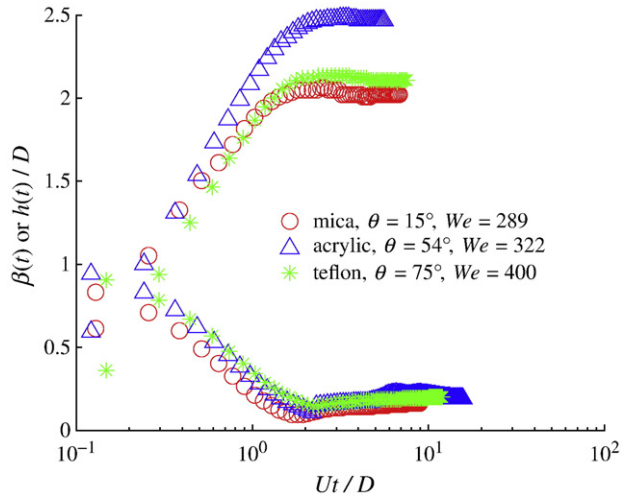

Fig. 23. Spreading diameter and centerline height for coating #4 on idealized surfaces for $We \sim 300$.

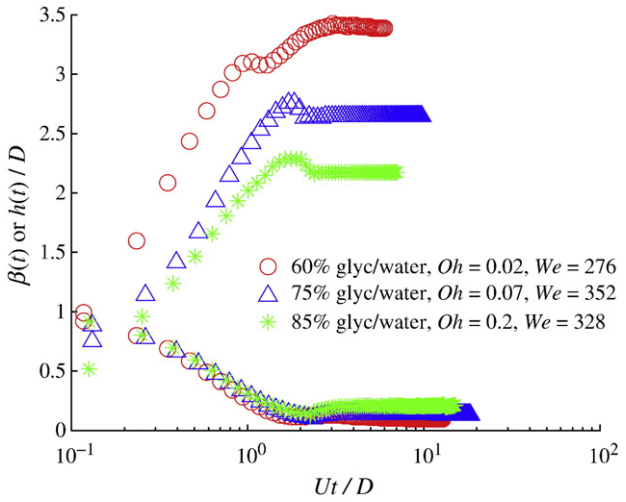

Fig. 24. Spreading diameter and centerline height for glycerol/water solutions on mica, $We \sim 300$. $Oh = 0.02$, 0.07, and 0.2 for 60, 75 and 85% glycerol/water. Note the halt in the contact line followed by further spreading. Influence of viscosity is obvious, minimizing viscosity enhances spreading during impact times $\sim D/U$.

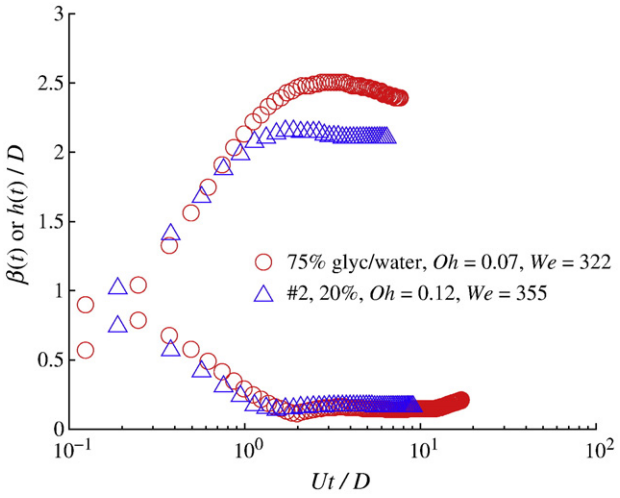

Fig. 26. Spreading diameter and centerline height for 75% glycerol/water solution and coating #2, 20% on teflon, $We \sim 300$. For 75% glycerol/water and #2 the $Oh \approx 0.07$ and 0.12, respectively. Slightly faster spread but only general behavior is identical.

compare our experimental results in the next section to two models that predict the maximum spreading diameter, β_{max}.

3.3.4. Study 4. Max diameter comparisons to models

The comparison of β_{max} extracted from the results shown herein and models of Mao et al. [30], Asai et al. [31], and Roisman [26] will demonstrate the utility of these models for colloidal dispersions. These two models are chosen here for comparison based on their simplicity and overall agreement with experimental data available in the literature. Fig. 27 compares the experimental versus predicted results using Eq. (15). It is apparent that the behavior follows reasonable agreement with predictions, within 12% when both glycerol/water and coatings are included together. When compared separately glycerol/water is within 9% and the coatings are within 13%. Comparing the data with the model of Mao, Eq. (14), gives slightly lower agreement with a total deviation of 13 % (11% glycerol/water and 13% for coatings) as seen in Fig. 28. The simpler model of Asai that avoids the inclusion of the contact angle still provides better agreement. The model of Roisman [26] shows better agreement for larger drops tested with approximately 8% error but deviates up to 50% for small drops at low *We* (Fig. 29). This was anticipated, since the viscous stresses in the rim are neglected in the development and deserves further attention. These coatings are viscous dominated in these early stages of impact and require further analysis. This is expected as we show in Fig. 30 how wettability has a negligible effect except for low *We* impacts (<2%) on the spreading and deposition during the initial stages of impact. Furthermore, in Fig. 31 we show that our experimental results confirm the work of Clanet et al. [27] and verify that in this highly viscous regime, $\beta_{max} \sim Re^{1/5}$.

4. Conclusion

A systematic study of droplet impact was conducted with both canonical Newtonian fluids with high viscosity and liquids relevant to the pharmaceutical industry. Such liquids contain large quantities of insoluble solids and result in an aqueous suspension. At viscosities on $\mathcal{O}$(10–100 cP) over a range of $We = \mathcal{O}(1–300)$, characteristic of spray coating conditions, we have demonstrated the outcome of drop impact results in spreading avoiding splash and rebound, with only minimal recession of the spreading diameter. The role of viscosity observed with and without colloids is the reason to explain the inhibition of splashing and rebounding. Furthermore, for intermediate

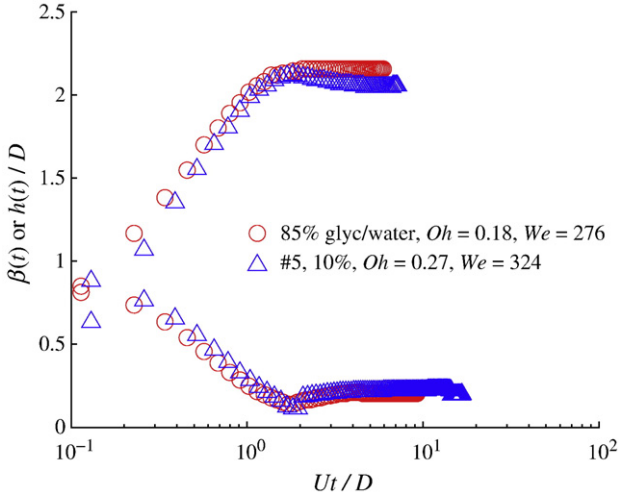

Fig. 25. Spreading diameter and centerline height for glycerol/water solutions on teflon, $We \sim 300$. For 85% glycerol/water and #5, 10% the $Oh \approx 0.2$, respectively. General behavior follows an exponentially decaying function.

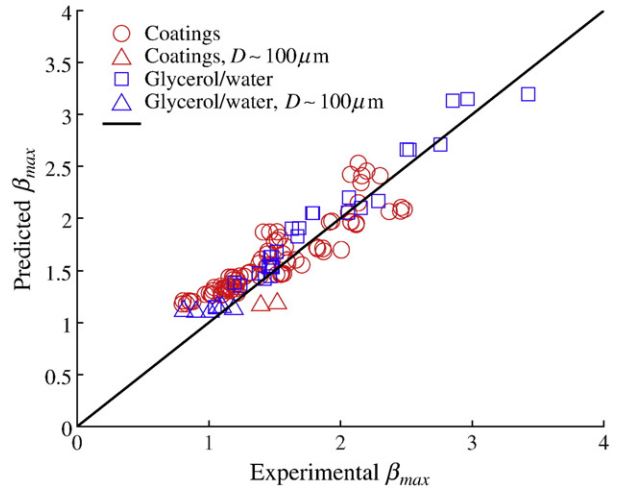

Fig. 27. Summary of β_{max} diameters for all fluids tested at a time of 1–4 Ut/D versus model of Asai, Eq. (15). Red circles indicate coating liquids and blue squares indicate glycerol/water mixtures.

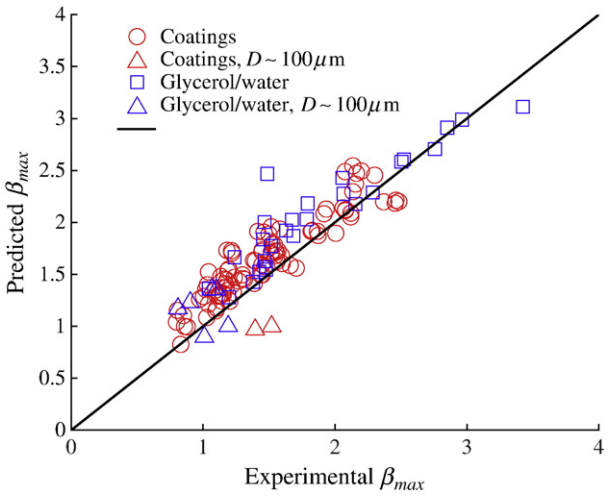

Fig. 28. Summary of β_{max} diameters at a time of 1–4 Ut/D versus model of Mao, Eq. (14). Red circles indicate coating liquids and blue squares indicate glycerol/water mixtures.

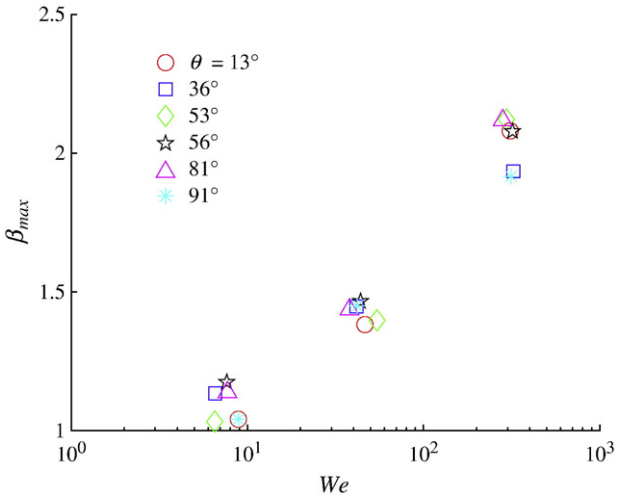

Fig. 30. Effect of wettability shown for β_{max}.

We, we found an interesting behavior that has not been characterized for pure liquids. In experiments with colloidal dispersions at $We \sim 30$, the height of the rim is found to increase linearly after the apex of the drop sinks below the rim as spreading is arrested which is also observed for comparable glycerol/water mixtures.

We confirm previous studies that during the initial stages of impact corresponding to $Ut/D \sim 1$–4, the spreading diameter is insensitive to wettability. Furthermore, we observe reasonable agreement with three existing models for β_{max} for all *We* studied. Despite reasonable agreement, the effect of the colloidal particles is not included and may assist in providing better agreement. The utility of the models of Asai et al. [31] and Mao et al. [30] still provides a robust model for first order approximations. The model of Roisman [26] provides the best correlation and points toward a more accurate method to modelling drop impact including the effect of particles. Additionally, we verify that the viscous regime obeys $\beta_{max} \sim Re^{1/5}$ even for the coating liquids studied herein.

This work stands to provide fundamental insight into aqueous colloidal suspension utilized in the pharmaceutical industry. We plan to investigate the impact of higher speed impacts of micron sized droplets and verify the results of the mm size experiments described herein. It is inconclusive to make any judgement about potential agreement. It is anticipated that small drops will be less likely to splash given the increased effect of viscosity, as characterized by larger values of *Oh* associated with smaller drops. The physical size of the drops should not change their behavior if the *Oh* is matched, unless there is another physical effect that we may not have taken into account. For small droplets, $\mathcal{O}(\mu m)$, shear rates may be larger, for a given *We* number, and therefore non-Newtonian effects on viscous dissipation will be a larger percentage of the energy partition. In order to keep *We* constant, we need to increase U^2 as D goes down. Moreover, since the shear rate is proportional to U/D, higher shear rates will be present and may induce different effects for comparable *We*. These topics will be a subject of future investigation.

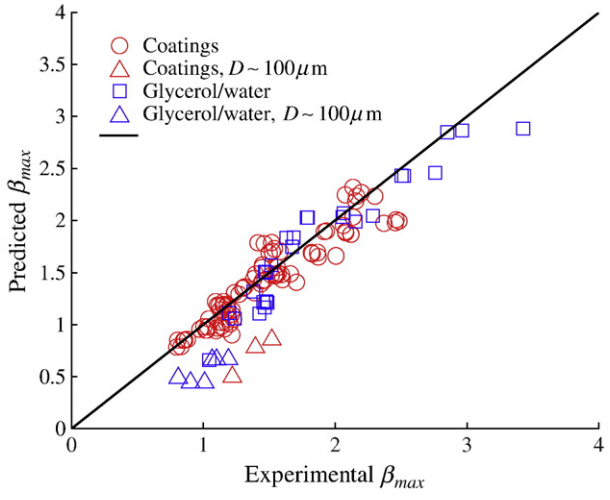

Fig. 29. Summary of β_{max} diameters at a time of 1–4 Ut/D versus model of Roisman, Eq. (16). Red circles indicate coating liquids and blue squares indicate glycerol/water mixtures.

Acknowledgements

The authors extend appreciation to Pankaj Doshi and Doug Kremer at Pfizer, Inc. for their support in this effort. We have also benefitted greatly from our collaborators at UCSD, Juan C. Lasheras and Katie Osterday. We appreciate Prof. Pozzo for the use of the rheometer. We are also grateful to Prof. J.C. Berg for the use of the contact angle measurement apparatus as well as his insightful comments during the preparation of this manuscript.

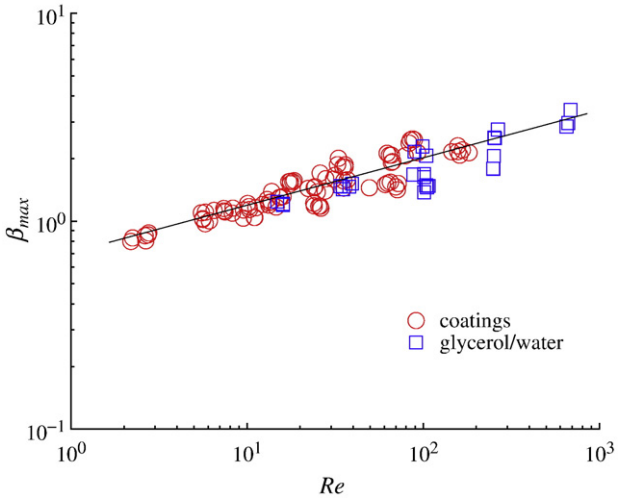

Fig. 31. β_{max} versus *Re* for coatings and glycerol/water mixtures. The points fit well to the solid line, $\beta_{max} \sim Re^{1/5}$.

Appendix A. Calculated dimensionless parameters

Table 4
Summary of calculated dimensionless parameters.

	2, 20%			4, 15%			5, 10%			5, 12%			5, 15%			60% glycerol			75% glycerol			85% glycerol		
	We	*Oh*	*Re*	*We*	*Oh*	*Re*	*We*	*Oh*	*Re*	*We*	*Oh*	*Re*	*We*	*Oh*	*Re*	*We*	*Oh*	*Re*	*We*	*Oh*	*Re*	*We*	*Oh*	*Re*
Acrylic	35	0.12	49	10	0.21	15	8	0.27	10	9	0.52	6	8	1.10	3	7	0.02	105	6	0.07	35	9	0.18	16
	72	0.12	71	32	0.21	26	44	0.27	24	49	0.52	14	62	1.10	7	37	0.02	249	50	0.07	101	40	0.18	35
	355	0.12	157	322	0.21	87	320	0.27	66	342	0.52	36	347	1.10	18	268	0.03	665	320	0.07	253	265	0.18	89
Mica	10	0.12	26	7	0.21	12	9	0.27	11	8	0.51	6	6	1.10	2	7	0.03	104	7	0.07	38	7	0.18	15
	59	0.12	65	55	0.21	35	42	0.27	24	65	0.51	16	77	1.10	8	38	0.02	252	39	0.07	88	52	0.18	39
	474	0.12	182	289	0.21	79	314	0.27	66	380	0.52	37	341	1.10	17	276	0.02	685	352	0.07	265	328	0.18	99
Teflon	8	0.12	24	8	0.21	13	7	0.27	10	9	0.50	6	5	1.10	2	7	0.02	107	8	0.07	101	9	0.18	16
	72	0.12	72	55	0.21	35	42	0.27	24	62	0.52	15	77	1.10	8	37	0.02	250	51	0.07	101	40	0.18	34
	355	0.12	157	400	0.21	93	324	0.27	67	338	0.52	35	378	1.10	18	262	0.03	650	322	0.07	255	364	0.18	104
3134	8	0.12	24	5	0.21	11	7	0.26	10	8	0.49	6	8	1.00	3									
	71	0.12	70	34	0.20	28	54	0.26	28	48	0.52	13	61	1.06	7									
	396	0.12	167	303	0.21	85	296	0.27	62	313	0.52	33	347	1.06	18									
3135	10	0.12	26	4	0.21	10	9	0.27	11	8	0.50	6	8	1.00	3									
	50	0.12	61	41	0.21	31	47	0.27	25	50	0.52	14	47	1.00	7									
	366	0.12	161	299	0.21	83	311	0.27	64	281	0.52	33	347	1.10	18									
3136	9	0.12	26	8	0.21	13	8	0.27	10	8	0.51	6	8	1.10	3									
	52	0.11	63	42	0.21	32	38	0.27	22	63	0.52	16	62	1.10	8									
	301	0.12	145	344	0.21	89	282	0.27	62	334	0.50	36	388	1.10	19									

References

[1] Worthington AM. On the forms assumed by drops of liquids falling vertically on a horizontal plate. Proc R Soc Lond03701662 1876;25:261–72.
[2] Bergeron V, Bonn D, Martin J, Vovelle L. Controlling droplet deposition with polymer additives. Nature 2000;405:772–5.
[3] Bartolo D, Boudaoud A, Narcy G, Bonn D. Dynamics of non-Newtonian droplets. Phys Rev Lett 2007;99:174502-1–4.
[4] Rioboo R, Tropea C. Outcomes from a drop impact on solid surfaces. Atomization Sprays 2001;11:155–65.
[5] Aliseda A, Hopfinger E, Lasheras J, Kremer D, Berchielli A, Connolly E. Atomization of viscous and non-Newtonian liquids by a coaxial, high-speed gas jet. Experiments and droplet size modeling. Int J Multiph Flow 2008;34:161–75.
[6] Rein M. Phenomena of liquid drop impact on solid and liquid surfaces. Fluid Dyn Res 1993;12:61–93.
[7] Yarin A. Drop impact dynamics: splashing, spreading, receding, bouncing. Annu Rev Fluid Mech 2006;38:159–92.
[8] Zhang X, Basaran O. Dynamic surface tension effects in impact of a drop with a solid surface. J Colloid Interface Sci 1997;187:166–78.
[9] Kannangara D, Zhang H, Shen W. Liquid–paper interactions during liquid drop impact and recoil on paper surfaces. Colloids Surf, A 2006;280:203–15.
[10] Daniel R, Berg J. Spreading on and penetration into thin, permeable print media: application to ink-jet printing. Advances in Colloids and Interface Science 2006: 439–69.
[11] Berg J. An introduction to interfaces and colloids: the bridge to nanoscience. World Scientific Publication Co.; 2010
[12] de Gennes P. Wetting: statics and dynamics. Rev Mod Phys 1985;57:827–63.
[13] Starov V, Kalinin V, Chen J. Spreading of liquid drops over dry surfaces. Adv Colloid Interface Sci 1994;50:187–221.
[14] Cox R. The dynamics of the spreading of liquids on a solid surface. Part 1. Viscous flow. J Fluid Mech 1986;168:169–94.
[15] Hocking L, Rivers A. The spreading of a drop by capillary action. J Fluid Mech 1982;121:425–42.
[16] Rioboo R, Marengo M, Tropea C. Time evolution of liquid drop impact onto solid, dry surfaces. Exp Fluids 2002;33:112–24.
[17] Middleman S. Modeling axisymmetric flows. London: Academic Press; 1995.
[18] Tanner L. The spreading of silicone oil drops on horizontal surfaces. J Phys D Appl Phys 1979;12.
[19] Rafaï S, Bonn D, Boudaoud A. Spreading of non-Newtonian fluids on hydrophilic surfaces. J Fluid Mech 2004;513:77–85.
[20] Dussan E. On the spreading of liquids on solid surfaces: static and dynamic contact lines. Annu Rev Fluid Mech 1979;11:371–400.
[21] Chandra S, Avedisian C. On the collision of a droplet with a solid surface. Proc R Soc Lond 1991;432:13–41.
[22] van Dam D, Clerc C. Experimental study of the impact of an ink-jet printed droplet on a solid surface. Phys Fluids 2004;16.
[23] Medhi-Nejad V, Mostaghimi J, Chandra S. Air bubble entrapment under an impacting droplet. Phys Fluids 2003;15:173–83.
[24] Attané P, Girard F, Morin V. An energy balance approach of the dynamics of drop impact on a solid surface. Phys Fluids 2007;19.
[25] Roisman I, Berberović E, Tropea C. Inertia dominated drop collisions. I. On the universal flow in the lamella. Phys Fluids 2009;21.
[26] Roisman I. Inertia dominated drop collisions. II. An analytical solution of the Navier–Stokes equations for a spreading viscous film. Phys Fluids 2009;21.
[27] Clanet C, Beguin C, Richard D, Quere D. Maximal deformation of an impacting drop. J Fluid Mech 2004;517:199–208.
[28] Scheller B, Bousfield D. Newtonian drop impact with a solid surface. AIChE Journal 1995;41.
[29] Pasandideh-Fard M, Qiao Y, Chandra S, Mostaghimi J. Capillary effects during droplet impact on a solid surface. Phys Fluids 1996;8:650–9.
[30] Mao T, Kuhn D, Tran H. Spread and rebound of liquid droplets upon impact on flat surfaces. AIChE J 1997;43:2169–79.
[31] Asai A, Shioya M, Hirasawa S, Okazaki T. Impact of an ink drop on paper. Journal of imaging science and technology. Imaging Science and Technology 1993;37.
[32] Roisman I, Rioboo R, Tropea C. Normal impact of a liquid drop on a dry surface: model for spreading and receding. Proc R Soc Lond 2002;458:1411–30.
[33] Bennett T, Poulikakos D. Splat-quench solidification: estimating the maximum spreading of a droplet impacting a solid surface. J Mater Sci 1993;28:963–70.
[34] Šikalo Š, Tropea C, Ganić E. Impact of droplets onto inclined surfaces. J Colloid Interface Sci 2005;286:661–9.
[35] Bakshi S, Roisman I, Tropea C. Investigations on the impact of a drop onto a small spherical target. Phys Fluids 2007;19.
[36] Harlow F, Shannon J. The splash of a liquid drop. J Appl Phys 1967;38:3855–66.
[37] Bechtel S, Bogy D, Talke F. Impact of a liquid drop against a flat surface. IBM J Res Develop 1981;25:963–71.
[38] Fukai J, Zhao Z, Poulikakos D, Megaridis C. Modeling of the deformation of a liquid drop impinging upon a flat surface. Phys Fluids 1993;5:2588–99.
[39] Fukai J, Shiiba Y, Yamamoto T, Miyatake O, Poulikakos D, Megaridis C, et al. Wetting effects on the spreading of a liquid droplet colliding with a flat surface: experiment and modeling. Phys Fluids 1995;7:236–47.
[40] Bussman M, Mostaghimi J, Chandra S. On a three-dimensional volume tracking model of droplet impact. Phys Fluids 1999;11:1406–17.
[41] Davidson M. Boundary integral predication of the spreading of an inviscid drop impacting on a solid surface. Chem Eng Sci 2000;55:1159–70.
[42] Pasandideh-Fard M, Chandra S, Mostaghimi J. A three-dimensional model of droplet impact and solidification. Int J Heat Mass Transfer 2002;45:2229–42.
[43] Quéré D. Wetting and roughness. Annu Rev Mater Res 2008;38:71–99.
[44] Richard D, Quéré D. Bouncing water drops. Europhys Lett 2000;50:769–75.
[45] Okumura K, Chevy F, Richard D, Quere D, Clanet C. Water spring: a model for bouncing drops. Europhys Lett 2003;62:237–43.
[46] Renardy Y, Popinet S, Duchemin L, Renardy M, Zaleski S, Josserand C, et al. Pyramidal and toroidal water drops after impact on a solid surface. J Fluid Mech 2003;484:69–83.
[47] Bayer I, Megaridis C. Contact angle dynamics in droplets impacting on flat surfaces with different wetting characteristics. J Fluid Mech 2006;558:415–49.
[48] Blake T, Haynes J. The kinetics of liquid/liquid displacement. J Colloid Interface Sci 1969;30.
[49] Kannan R, Sivakumar D. Impact of liquid drops on a rough surface comprising microgrooves. Exp Fluids 2008;44:927–38.
[50] Kim H-Y, Chun J-H. The recoiling of liquid droplets upon collision with solid surfaces. Phys Fluids 2001;13:643–59.
[51] Caviezel D, Narayanan C, Lakehal D. Adherence and bouncing of liquid droplets impacting on dry surfaces. Microfluid Nanofluid 2008;5:469–78.
[52] Heymann F. High-speed impact between a liquid drop and a solid surface. J Appl Phys 1969;40:5113–22.
[53] Lesser M. Analytic solutions of liquid-drop impact problems. Proc R Soc Lond 1981;377:289–308.
[54] Lesser M, Field J. The impact of compressible liquids. Annu Rev Fluid Mech 1983;15:97–122.

[55] Dear J, Field J. High-speed photography of surface geometry effects in liquid/solid impact. J Appl Phys 1988;63:1015–21.
[56] Field J, Dear J, Ogren J. The effects of target compliance on liquid drop impact. J Appl Phys 1989;65:533–40.
[57] Stow C, Hadfield M. An experimental investigation of fluid flow resulting from the impact of a water drop with an unyielding dry surface. Proc R Soc Lond 1981;373: 419–41.
[58] Mundo C, Sommerfeld M, Tropea C. Droplet–wall collisions: experimental studies of the deformation and breakup process. Int J Multiph Flow 1995;2:151–73.
[59] Range K, Feuillebois F. Influence of surface roughness on liquid drop impact. J Colloid Interface Sci 1998;203:16–30.
[60] Yarin A, Weiss D. Impact of drops on solid surfaces: self-similar capillary waves, and splashing as a new type of kinematic discontinuity. J Fluid Mech 1995;283: 141–73.
[61] Cohen RD. Shattering of a liquid drop due to impact. Proc R Soc Lond 1991;435: 483–503.
[62] Bhola R, Chandra S. Parameters controlling solidification of molten wax droplets falling on a solid surface. J Mater Sci 1999;34:4883–94.
[63] Aziz S, Chandra S. Impact, recoil and splashing of molten metal droplets. Int J Heat Mass Transfer 2000;43:2841–57.
[64] Bussmann M, Chandra S, Mostaghimi J. Modeling the splash of a droplet impacting a solid surface. Phys Fluids 2000;12:3121–32.
[65] Bird J, Tsai SSH, Stone H. Inclined to splash: triggering and inhibiting a splash with tangential velocity. New Journal of Physics 2009;11.
[66] Xu L, Barcos L, Nagel S. Splashing of liquids: interplay of surface roughness with surrounding gas. Physical Review E 2007;76.
[67] L. Xu, L. Barcos, S. Nagel, Splashing of liquids: interplay of surface roughness with surrounding gas. Physical Review E. 76.
[68] Mandre S, Mani M, Brennner M. Precursors to splashing of liquid drops on a solid surface. Phys Rev Lett 2009;102:134502.
[69] Schiaffino S, Sonin AA. Molten droplet deposition and solidification at low Weber numbers. Physics of Fluids 1997;11:3172–87, doi:10.1063/1.869434 URL http://link.aip.org/link/?PHF/9/3172/1.
[70] Attinger D, Zhao A, Poulikakos D. An experimental study of molten microdroplet surface deposition and solidification: transient behavior and wetting angle dynamics. ASME 2000.
[71] Chen A, Basaran O. A new method for significantly reducing drop radius without reducing nozzle radius in drop-on-demand drop production. Physics of Fluids Letters 2002;14.
[72] Dong H, Carr W, Morris J. Visualization of drop-on-demand inkjet: drop formation and deposition. Rev Sci Instrum 2006;77.
[73] Shore H, Harrison G. The effect of added polymers on the formation of drops ejected from a nozzle. Phys Fluids 2005;17.
[74] Son Y, Kim C, Yang D, Ahn D. Spreading of an inkjet droplet on a solid surface with a controlled contact angle at low Weber and Reynolds numbers. Langmuir 2008;24:2900–7.
[75] Son Y, Kim C. Spreading of inkjet droplet of non-Newtonian fluid on solid surface with controlled contact angle at low Weber and Reynolds numbers. J Non-Newtonian Fluid Mech 2009;162:78–87.
[76] Toivakka M. Numerical investigation of droplet impact spreading in spray coating of paper. Spring Advanced Coating Fundamentals Symposium; 2003.
[77] Mourougou-Candoni N, Prunet-Foch B, Legay F, Vignes-Adler M, Wong K. Influence of dynamic surface tension on the spreading of surfactant solution droplets impacting onto a low-surface-energy solid substrate. J Colloid Interface Sci 1997;192:129–41.
[78] Mourougou-Candoni N, Prunet-Foch B, Legay F, Vignes-Adler M. Retraction phenomena of surfactant solution drops upon impact on a solid substrate of low surface energy. Langmuir 1999;15:6563–74.
[79] Prunet-Foch B, Legay F, Vignes-Adler M, Delmotte C. Impacting emulsion drop on a steel plate: influence of the solid substrate. J Colloid Interface Sci 1998;199: 151–68.
[80] Cooper-White J, Crooks R, Boger D. A drop impact study of worm-like viscoelastic surfactant solutions. Colloids Surf, A 2002;210:105–23.
[81] Cooper-White J, Crooks R, Chockalingham K, Boger D. Dynamics of polymer–surfactant complexes: elongational properties and drop impact behavior. Ind Eng Chem Res 2002;41:6443–59.
[82] Rozhkov A, Prunet-Foch B, Vignes-Adler M. Impact of drops of polymer solutions on small targets. Phys Fluids 2003;15:2006–19.
[83] Rozhkov A, Prunet-Foch B, Vignes-Adler M. Dynamics and disintegration of drops of polymeric liquids. J Non-Newtonian Fluid Mech 2006;134:44–55.
[84] Nicolas M. Spreading of a drop of neutrally buoyant suspension. J Fluid Mech 2005;545:271–80.
[85] Nigen S. Experimental investigation of the impact of an (apparent) yield–stress material. Atomization Sprays 2005;15:103–17.
[86] Klimek R, Wright R. Spotlight-8 image analysis software. NASA TM 214084 2005. http://microgravity.grc.nasa.gov/spotlight/.
[87] Dong H, Carr W, Bucknall D, Morris J. Temporally-resolved inkjet drop impaction on surfaces. AIChE Journal 2007;53.